Partitioning gene-level contributions to complex-trait heritability by allele frequency identifies disease-relevant genes

Authors

Kathryn S. Burch, Kangcheng Hou, Yi Ding, Yifei Wang, Steven Gazal, Huwenbo Shi, Bogdan Pasaniuc

Correspondence

kathrynburch@ucla.edu (K.S.B.), pasaniuc@ucla.edu (B.P.)

Burch et al., 2022, The American Journal of Human Genetics *109*, 692–709
April 7, 2022
https://doi.org/10.1016/j.ajhg.2022.02.012

CellPress

ARTICLE

Partitioning gene-level contributions to complex-trait heritability by allele frequency identifies disease-relevant genes

Kathryn S. Burch,[1,8,9,*] Kangcheng Hou,[1,8,9] Yi Ding,[1,8] Yifei Wang,[2] Steven Gazal,[3] Huwenbo Shi,[4,5,6] and Bogdan Pasaniuc[1,2,7,8,*]

Summary

Recent works have shown that SNP heritability—which is dominated by low-effect common variants—may not be the most relevant quantity for localizing high-effect/critical disease genes. Here, we introduce methods to estimate the proportion of phenotypic variance explained by a given assignment of SNPs to a single gene ("gene-level heritability"). We partition gene-level heritability by minor allele frequency (MAF) to find genes whose gene-level heritability is explained exclusively by "low-frequency/rare" variants ($0.5\% \leq \text{MAF} < 1\%$). Applying our method to ~16K protein-coding genes and 25 quantitative traits in the UK Biobank (N = 290K "White British"), we find that, on average across traits, ~2.5% of nonzero-heritability genes have a rare-variant component and only ~0.8% (327 gene-trait pairs) have heritability exclusively from rare variants. Of these 327 gene-trait pairs, 114 (35%) were not detected by existing gene-level association testing methods. The additional genes we identify are significantly enriched for known disease genes, and we find several examples of genes that have been previously implicated in phenotypically related Mendelian disorders. Notably, the rare-variant component of gene-level heritability exhibits trends different from those of common-variant gene-level heritability. For example, while total gene-level heritability increases with gene length, the rare-variant component is significantly larger among shorter genes; the cumulative distributions of gene-level heritability also vary across traits and reveal differences in the relative contributions of rare/common variants to overall gene-level polygenicity. While nonzero gene-level heritability does not imply causality, if interpreted in the correct context, gene-level heritability can reveal useful insights into complex-trait genetic architecture.

Introduction

It is well established that complex-trait SNP-heritability is enriched in regulatory regions.[1–3] However, for most complex traits, fundamental characteristics of genetic architecture—for example, the number of variants/genes with nonzero effects (polygenicity), the number of genes regulated by local versus distal variants, and the relative contributions of rare versus common variants to gene expression and phenotype—remain actively debated.[4–12]

Because SNP-heritability is overwhelmingly driven by common variants of low effect—individual rare variants with large per-allele effects contribute very little to population-level phenotypic variance[13,14]—whether the largest heritability enrichments localize the most clinically relevant regions and/or genes for a trait is unclear. For example, a recent study found that most complex-trait SNP heritability mediated via the *cis*-genetic component of expression is explained by genes that individually have low *cis*-heritability of expression.[15] Another study found that extreme complex-trait polygenicity may be explained in large part by negative/stabilizing selection, which by purging high-effect alleles from the population, "flattens" the distribution of SNP heritability across common variants genome wide.[16,17] If the most critical genes for a trait are not necessarily localized by enrichments of total heritability,[15,16,18,19] genes identified via heritability enrichments or overlaps between genome-wide association studies (GWASs) and expression quantitative trait loci[20,21] become even more challenging to interpret. Gene-based association tests that aggregate signal from multiple rare variants—for example, burden tests and sequence-based association tests (SKATs)—can increase power under different genetic-architecture scenarios.[22–30] However, such methods are generally designed to test for only rare-variant association or the combined effects of common and rare variants and thus are not ideal for parsing the relative contributions of rare/common variants to the heritability of a single gene.

Here, we define and aim to estimate a quantity we call "gene-level heritability" (h^2_{gene})—the proportion of phenotypic variance explained by the additive effects of a given set of variants assigned to a gene of interest. The key challenge in estimating gene-level heritability lies in the

[1]Bioinformatics Interdepartmental Program, University of California, Los Angeles, Los Angeles, CA 90095, USA; [2]Department of Pathology and Laboratory Medicine, David Geffen School of Medicine at University of California, Los Angeles, Los Angeles, CA 90095, USA; [3]Center for Genetic Epidemiology, Department of Population and Public Health Sciences, Keck School of Medicine, University of Southern California, Los Angeles, CA 90033, USA; [4]Department of Epidemiology, Harvard T.H. Chan School of Public Health, Boston, MA 02115, USA; [5]Program in Medical and Population Genetics, Broad Institute of MIT and Harvard, Cambridge, MA 02142, USA; [6]OMNI Bioinformatics, Genentech, 1 DNA Way, South San Francisco, CA 94080, USA; [7]Department of Human Genetics, David Geffen School of Medicine at University of California, Los Angeles, Los Angeles, CA 90095, USA; [8]Department of Computational Medicine, David Geffen School of Medicine at University of California, Los Angeles, Los Angeles, CA 90095, USA
[9]These authors contributed equally
*Correspondence: kathrynburch@ucla.edu (K.S.B.), pasaniuc@ucla.edu (B.P.)
https://doi.org/10.1016/j.ajhg.2022.02.012.

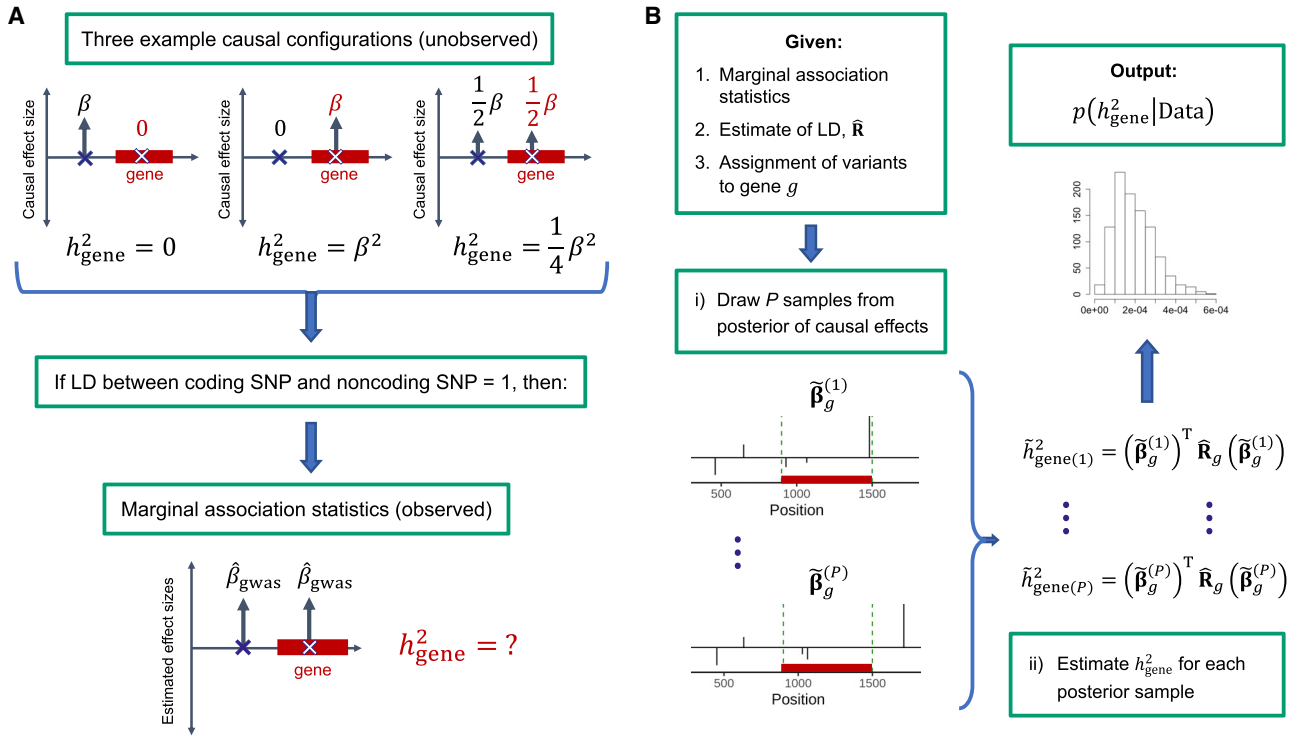

Figure 1. Overview

(A) Toy example with two variants, one of which is assigned to the gene of interest. The top row depicts three example causal configurations corresponding to three different gene-level heritabilities (0, β^2, and $\beta^2/4$); for simplicity of presentation, we assume the genotypes are standardized to have variance 1 in the population (material and methods). All three causal configurations yield the same expected marginal association statistics.

(B) Given marginal association statistics, an estimate of LD, and an assignment of variants to the gene of interest, our method involves (1) sampling from the posterior of the causal effect sizes (assuming a sparse prior) to capture causal-effect uncertainty and then (2) estimating gene-level heritability for each posterior sample to approximate the posterior distribution of gene-level heritability.

uncertainty about which variants are causal and what their causal effect sizes are, both of which increase as the strength of linkage disequilibrium (LD) in the region increases and as GWAS sample size decreases.[31] Consider a toy example in which a variant in the gene of interest is in perfect LD with a second variant adjacent to the gene and the observed data are GWAS marginal association statistics and LD (Figure 1A). Without additional information, it is impossible to elucidate the underlying causal configuration. Even if the LD is 0.9 instead of 1, if this GWAS has 90% power to identify the region, correctly rejecting the null hypothesis for the non-causal variant would require a sample size $\geq 4\times$ that of the original GWAS.[31] Because each causal configuration can yield a different gene-level heritability (with or without minor allele frequency [MAF] partitioning), randomly selecting one possible configuration (e.g., using variable selection methods such as the Lasso[32]) can yield inaccurate/misleading estimates. Estimators for the SNP heritability of a single region would most likely be inflated if applied as-is to genes because of LD between variants in the region of interest and the adjacent regions.[18,33–35] Methods for partitioning genome-wide SNP heritability are also ill-suited to our goals, as they make distributional assumptions on the causal effects, which (1) limit power to detect enrichment in small categories of variants (<1% of the genome) and/or (2) may not apply equally to rare and common variants.[3,36–41]

We propose an approach to estimating h^2_{gene} that captures causal-effect uncertainty by sampling from the posterior distribution of the causal effect sizes within a probabilistic fine-mapping framework.[42] We use the samples from the posterior of the causal effects to approximate the posterior distribution of h^2_{gene} (Figure 1B), from which one can compute various summary statistics of interest. For each gene, we report the posterior mean, denoted $\widehat{h}^2_{\text{gene}}$, and a ρ-level credible interval, or ρ-CI, defined as the central interval containing the true gene-level heritability with probability ρ (material and methods). We confirm in simulations that accounting for uncertainty in the estimated causal effects significantly reduces the bias of $\widehat{h}^2_{\text{gene}}$ and that both $\widehat{h}^2_{\text{gene}}$ and ρ-CIs are robust to causal effect sizes, gene length, allele frequencies of causal variants, and the strength of local LD. Under the (potentially strong) assumption that there is zero covariance between causal effects of different variants,[43–46] total gene-level heritability can be expressed as $h^2_{\text{gene,t}} = h^2_{\text{gene,r}} + h^2_{\text{gene,lf}} + h^2_{\text{gene,c}}$ (material and methods), where the terms refer to the components of $h^2_{\text{gene,t}}$ explained by rare (MAF $< 1\%$), low-frequency ($1\% \leq$MAF $< 5\%$), and common (MAF$\geq 5\%$) variants, respectively. We apply the same approach to estimate the posterior distributions of

$h^2_{\text{gene,r}}$, $h^2_{\text{gene,lf}}$, and $h^2_{\text{gene,c}}$ and observe similar trends and levels of accuracy. (While there are many definitions of "rare" in the literature, we use $0.5\% \leq \text{MAF} < 1\%$ in the present work because we analyze imputed genotypes.)

Applying our approach to 15,770 protein-coding genes and 25 quantitative traits in the UK Biobank[47] (N = 290K self-reported "White British," MAF > 0.5%), we confirm that $h^2_{\text{gene,t}}$ is indeed dominated by $h^2_{\text{gene,c}}$. On average across traits, among genes with $h^2_{\text{gene,t}}$ 90%-CI > 0 ("nonzero-heritability genes"), 92% (SD 1%) have nonzero common-variant heritability, and 76% (SD 1%) have nonzero heritability exclusively from common variants ($h^2_{\text{gene,t}} \approx h^2_{\text{gene,c}}$). In contrast, only 2.5% (SD 0.6%) of nonzero-heritability genes, averaged across traits, have nonzero rare-variant heritability, and a mere 0.8% (SD 0.4%) have nonzero heritability exclusively from rare variants ($h^2_{\text{gene,t}} \approx h^2_{\text{gene,r}}$). The 2.5% of genes with $h^2_{\text{gene,r}}$ 90%-CI > 0 is enriched for Mendelian-disorder genes and genes intolerant to loss of function (probability of loss-of-function [LoF] intolerance[48,49] > 0.9), whereas the 0.8% of genes with $h^2_{\text{gene,t}} \approx h^2_{\text{gene,r}}$ (327 gene-trait pairs in total) is enriched only for LoF-intolerant genes. However, in both gene sets—genes with rare-variant heritability and genes with exclusively rare-variant heritability—the top genes (rank ordered by $\widehat{h}^2_{\text{gene,r}}$) contain many examples of genes with known roles in phenotypically similar Mendelian disorders or other congenital growth and developmental disorders.

We emphasize that gene-level heritability is not an intrinsic property of a trait or gene but rather, like all "types" of heritability, a function of the environmental variance in the specific population being studied.[50,51] Because allele frequencies are population specific, and causal alleles and their effect sizes can also differ across populations (e.g., due to population-specific environmental exposures),[52,53] estimates of total and MAF-partitioned gene-level heritability—like all partitioned heritability estimates—are only meaningful when considered in the populations in which they were measured. The real-data results presented here are therefore specific to a population of "White British" individuals living in the UK. In addition, nonzero-heritability genes must not be interpreted as biologically causal without additional validation, as nonzero heritability indicates association not causality.[51] Nevertheless, our results are consistent with the hypothesis that a sizable amount of complex-trait variation is driven by dysregulation of genes that—if completely disrupted—cause phenotypically similar monogenic disorders and/or systemic congenital and developmental disorders.[54] Because genes can be disrupted/dysregulated by a combination of common and rare variants, $h^2_{\text{gene,r}}$ should be considered alongside common-variant heritability enrichments if one is interested in identifying high-impact disease genes. While we restrict our analyses to genes (gene body ± 10-kb window), our method can be applied to any small annotation of interest (e.g., enhancers, a set of genes involved in a pathway). Similar approaches have also been applied for analysis of temporal trends in additive genetic variance (e.g., in livestock breeding programs).[55,56]

Material and Methods

Model and definitions of estimands

We model the phenotype of a given individual by using a standard linear model, $y = \mathbf{x}^{\mathrm{T}}\boldsymbol{\beta} + \varepsilon$, where $\mathbf{x}^{\mathrm{T}} = (x_1 \ldots x_M)^{\mathrm{T}}$ is the vector of the individual's genotypes at M variants, assumed to be standardized in the population such that $\mathbb{E}[x_i] = 0$ and $var[x_i] = 1$ for $i = 1, \ldots, M$; $\boldsymbol{\beta}$ is the $M \times 1$ vector of corresponding standardized causal effect sizes; and $\varepsilon \sim N(0, \sigma^2_\varepsilon)$ is environmental noise. The individual's standardized genotype at the i-th variant is $x_i = (g_i - 2f_i)/\sqrt{2f_i(1-f_i)}$ where $g_i \in \{0, 1, 2\}$ is the number of copies of the effect allele carried by the individual at the i-th variant and f_i is the allele frequency of the effect allele in the population. Under this model, LD between variants i and j is defined as $r_{ij} \equiv cov[x_i, x_j] = \mathbb{E}[x_i x_j]$ and the full LD matrix for all M variants is $\mathbf{R} \equiv cov[\mathbf{x}^{\mathrm{T}}]$. We assume that the phenotype is also standardized in the population such that $\mathbb{E}[y] = 0$, $var[y] = 1$.

Let $p_{\text{causal}} \in [0, 1]$ such that $M \times p_{\text{causal}}$ is the total number of causal variants. We assume the causal effect of the i-th variant is distributed $\beta_i \sim N(0,\ h^2_G/(Mp_{\text{causal}}))$ with probability p_{causal} or $\beta_i = 0$ with probability $1 - p_{\text{causal}}$, where h^2_G, total SNP heritability, is the proportion of phenotypic variance explained by all M variants. Using the law of total variance,

$$
\begin{aligned}
h^2_{\mathrm{G}} &\equiv \frac{var[\mathbf{x}^{\mathrm{T}}\boldsymbol{\beta}]}{var[y]} \\
&= \mathbb{E}_{\boldsymbol{\beta}}\left[var\left[\mathbf{x}^{\mathrm{T}}\boldsymbol{\beta}|\boldsymbol{\beta}\right]\right] + var_{\boldsymbol{\beta}}\left[\mathbb{E}\left[\mathbf{x}^{\mathrm{T}}\boldsymbol{\beta}|\boldsymbol{\beta}\right]\right] \\
&= \mathbb{E}_{\boldsymbol{\beta}}\left[\boldsymbol{\beta}^{\mathrm{T}} var\left[\mathbf{x}^{\mathrm{T}}\right]\boldsymbol{\beta}\right] + var_{\boldsymbol{\beta}}\left[\mathbb{E}\left[\mathbf{x}^{\mathrm{T}}\right]\boldsymbol{\beta}\right] \\
&= \mathbb{E}_{\boldsymbol{\beta}}\left[\boldsymbol{\beta}^{\mathrm{T}}\mathbf{R}\boldsymbol{\beta}\right] + var_{\boldsymbol{\beta}}[0] \\
&= \mathbb{E}_{\boldsymbol{\beta}}\left[\boldsymbol{\beta}^{\mathrm{T}}\mathbf{R}\boldsymbol{\beta}\right].
\end{aligned}
$$

Let g index a gene of interest. Given an assignment of m_g variants to gene g, let $\mathbf{x}^{\mathrm{T}}_g$ be the $m_g \times 1$ vector of genotypes at this set of variants and let $\mathbf{x}^{\mathrm{T}}_{g'}$ be the genotypes of the remaining $M - m_g$ variants. We can rewrite the total SNP heritability of the trait in terms of gene g as

$$
\begin{aligned}
h^2_{\mathrm{G}} &= \mathrm{Var}\left[\mathbf{x}^{\mathrm{T}}_g\boldsymbol{\beta}_g + \mathbf{x}^{\mathrm{T}}_{g'}\boldsymbol{\beta}_{g'}\right] = \mathrm{Var}\left[\mathbf{x}^{\mathrm{T}}_g\boldsymbol{\beta}_g\right] + \mathrm{Var}\left[\mathbf{x}^{\mathrm{T}}_{g'}\boldsymbol{\beta}_{g'}\right] + 2\mathrm{Cov}\left[\mathbf{x}^{\mathrm{T}}_g\boldsymbol{\beta}_g, \mathbf{x}^{\mathrm{T}}_{g'}\boldsymbol{\beta}_{g'}\right] \\
&= \mathrm{E}_{\boldsymbol{\beta}}\left[\boldsymbol{\beta}^{\mathrm{T}}_g\mathbf{R}_g\boldsymbol{\beta}_g\right] + \mathrm{E}_{\boldsymbol{\beta}}\left[\boldsymbol{\beta}^{\mathrm{T}}_{g'}\mathbf{R}_{g'}\boldsymbol{\beta}_{g'}\right] + 2\left[\mathrm{E}\left[\left(\mathbf{x}^{\mathrm{T}}_g\boldsymbol{\beta}_g\right)\left(\mathbf{x}^{\mathrm{T}}_{g'}\boldsymbol{\beta}_{g'}\right)\right] - \mathrm{E}\left[\mathbf{x}^{\mathrm{T}}_g\boldsymbol{\beta}_g\right]\mathrm{E}\left[\mathbf{x}^{\mathrm{T}}_{g'}\boldsymbol{\beta}_{g'}\right]\right] \\
&= \mathrm{E}_{\boldsymbol{\beta}}\left[\boldsymbol{\beta}^{\mathrm{T}}_g\mathbf{R}_g\boldsymbol{\beta}_g\right] + \mathrm{E}_{\boldsymbol{\beta}}\left[\boldsymbol{\beta}^{\mathrm{T}}_{g'}\mathbf{R}_{g'}\boldsymbol{\beta}_{g'}\right] + 2\mathrm{E}_{\boldsymbol{\beta}}\left[\mathrm{E}\left[\left(\mathbf{x}^{\mathrm{T}}_g\boldsymbol{\beta}_g\right)\left(\boldsymbol{\beta}^{\mathrm{T}}_{g'}\mathbf{x}_{g'}\right)\middle|\boldsymbol{\beta}\right]\right] - 2\mathrm{E}_{\boldsymbol{\beta}}\left[\mathrm{E}\left(\mathbf{x}^{\mathrm{T}}_g\boldsymbol{\beta}_g\middle|\boldsymbol{\beta}\right)\right]\mathrm{E}_{\boldsymbol{\beta}}\left[\mathrm{E}\left(\mathbf{x}^{\mathrm{T}}_{g'}\boldsymbol{\beta}_{g'}\middle|\boldsymbol{\beta}\right)\right] \\
&= \mathrm{E}_{\boldsymbol{\beta}}\left[\boldsymbol{\beta}^{\mathrm{T}}_g\mathbf{R}_g\boldsymbol{\beta}_g\right] + \mathrm{E}_{\boldsymbol{\beta}}\left[\boldsymbol{\beta}^{\mathrm{T}}_{g'}\mathbf{R}_{g'}\boldsymbol{\beta}_{g'}\right] + 2\mathrm{E}_{\boldsymbol{\beta}}\left[\boldsymbol{\beta}_g\boldsymbol{\beta}^{\mathrm{T}}_{g'}\mathrm{E}\left[\mathbf{x}_{g'}\mathbf{x}^{\mathrm{T}}_g\right]\right] - 0 \\
&= \mathrm{E}_{\boldsymbol{\beta}}\left[\boldsymbol{\beta}^{\mathrm{T}}_g\mathbf{R}_g\boldsymbol{\beta}_g\right] + \mathrm{E}_{\boldsymbol{\beta}}\left[\boldsymbol{\beta}^{\mathrm{T}}_{g'}\mathbf{R}_{g'}\boldsymbol{\beta}_{g'}\right] + 2\mathrm{E}_{\boldsymbol{\beta}}\left[\boldsymbol{\beta}_g\boldsymbol{\beta}^{\mathrm{T}}_{g'}\right]\mathrm{E}_{\mathbf{x}}\left[\mathbf{x}_{g'}\mathbf{x}^{\mathrm{T}}_g\right]
\end{aligned}
$$

where the fourth line follows from the law of total expectation. If we additionally assume that $cov[\beta_i, \beta_j] = 0$ for all $i \neq j$, then $\mathbb{E}[\boldsymbol{\beta}_{(g)}\boldsymbol{\beta}_{(g')}^{\mathrm{T}}] = cov[\boldsymbol{\beta}_{(g)}, \boldsymbol{\beta}_{(g')}] = 0$, which simplifies the above equation to

$$h_{\mathrm{G}}^2 = \mathbb{E}_{\boldsymbol{\beta}}\left[\boldsymbol{\beta}_g^{\mathrm{T}}\mathbf{R}_g\boldsymbol{\beta}_g\right] + \mathbb{E}_{\boldsymbol{\beta}}\left[\boldsymbol{\beta}_{g'}^{\mathrm{T}}\mathbf{R}_{g'}\boldsymbol{\beta}_{g'}\right].$$

We refer to the first term, the component of heritability attributable to the causal effects in gene g, as "total gene-level heritability":

$$h_{\mathrm{gene,t}}^2 = \mathbb{E}_{\boldsymbol{\beta}}\left[\boldsymbol{\beta}_g^{\mathrm{T}}\mathbf{R}_g\boldsymbol{\beta}_g\right].$$

Using the same assumptions as above, we can partition the variants in gene g by MAF such that

$$h_{\mathrm{gene,t}}^2 = h_{\mathrm{gene,r}}^2 + h_{\mathrm{gene,lf}}^2 + h_{\mathrm{gene,c}}^2$$

where $h_{\mathrm{gene,r}}^2$, $h_{\mathrm{gene,lf}}^2$, and $h_{\mathrm{gene,c}}^2$ are the components of $h_{\mathrm{gene,t}}^2$ attributable to the causal effects of rare (MAF $<$ 0.01), low-frequency (0.01 $\leq$ MAF $<$ 0.05), and common (MAF $\geq$ 0.05) variants, respectively. The estimands of interest in this work are the four terms in $h_{\mathrm{gene,t}}^2 = h_{\mathrm{gene,r}}^2 + h_{\mathrm{gene,lf}}^2 + h_{\mathrm{gene,c}}^2$.

Note on the impact of the assumption of zero covariance between causal effects at different loci

Although it is common for post-GWAS analysis methods to assume that $cov[\beta_i, \beta_j] = 0$ for all $i \neq j$ to facilitate inference, this may in fact be a relatively strong assumption on the underlying genetic architecture.[43–46] If this assumption is unmet, the equation for total SNP heritability retains its covariance term, i.e.,

$$\begin{aligned} h_{\mathrm{G}}^2 &= \mathrm{E}_{\boldsymbol{\beta}}\left[\boldsymbol{\beta}_g^{\mathrm{T}}\mathbf{R}_g\boldsymbol{\beta}_g\right] + \mathrm{E}_{\boldsymbol{\beta}}\left[\boldsymbol{\beta}_{g'}^{\mathrm{T}}\mathbf{R}_{g'}\boldsymbol{\beta}_{g'}\right] + 2\mathrm{E}_{\boldsymbol{\beta}}\left[\boldsymbol{\beta}_g\boldsymbol{\beta}_{g'}^{\mathrm{T}}\right]\mathrm{E}_{\mathbf{x}}\left[\mathbf{x}_{g'}\mathbf{x}_g^{\mathrm{T}}\right] \\ &= h_{\mathrm{gene}}^2 + h_{\mathrm{gene'}}^2 + 2\mathrm{E}_{\boldsymbol{\beta}}\left[\boldsymbol{\beta}_g\boldsymbol{\beta}_{g'}^{\mathrm{T}}\right]\mathrm{E}_{\mathbf{x}}\left[\mathbf{x}_{g'}\mathbf{x}_g^{\mathrm{T}}\right]. \end{aligned}$$

The interpretation of our definition of gene-level heritability, $h_{\mathrm{gene}}^2 = \mathbb{E}_{\boldsymbol{\beta}}[\boldsymbol{\beta}_g^{\mathrm{T}}\mathbf{R}_g\boldsymbol{\beta}_g]$, can then be thought of as the component of heritability that is "uniquely assignable" to the gene of interest. See discussion for additional commentary on the impact of nonzero causal-effect covariance on estimates of gene-level heritability. We also note that alternative assumptions yield different models for analyses of genomic variance (e.g., models of temporal trends in additive genetic variance[55,56]).

Estimating the posterior distribution of gene-level heritability

Because we have neither the "true" causal effect sizes, $\boldsymbol{\beta}$, nor the population LD, $\mathbf{R}$, we must estimate both from data. We consider one approximately independent LD block at a time. Given a GWAS of N individuals, let $\mathbf{X} = [\mathbf{x}_1^{\mathrm{T}}, \ldots, \mathbf{x}_N^{\mathrm{T}}]^{\mathrm{T}}$ be the $N \times M$ matrix of standardized genotypes measured at M variants, let $\mathbf{y} = (y_1, \ldots, y_N)^{\mathrm{T}}$ be an $N \times 1$ vector of phenotypes, and let $\boldsymbol{\epsilon} \sim MVN(0, \sigma_e^2\mathbf{I}_N)$ be environmental noise.

It is often the case that individual-level genotype data are inaccessible for privacy or logistical reasons. However, GWAS summary statistics—estimates of the causal effects and their standard errors—are publicly available for thousands of traits. Ordinary least-squares (OLS) estimates of the causal effects are often provided, defined as

$$\widehat{\boldsymbol{\beta}}_{\mathrm{GWAS}} = \frac{1}{N}\mathbf{X}^{\mathrm{T}}\mathbf{y} = \frac{1}{N}\mathbf{X}^{\mathrm{T}}(\mathbf{X}\boldsymbol{\beta} + \boldsymbol{\epsilon}) = \frac{1}{N}\mathbf{X}^{\mathrm{T}}\mathbf{X}\boldsymbol{\beta} + \frac{1}{N}\mathbf{X}^{\mathrm{T}}\boldsymbol{\epsilon}.$$

It follows that

$$p(\widehat{\boldsymbol{\beta}}_{\mathrm{GWAS}}|\boldsymbol{\beta}, \widehat{\mathbf{R}}, \sigma_e^2) \sim MVN\left(\widehat{\mathbf{R}}\boldsymbol{\beta}, \frac{\sigma_e^2}{N}\widehat{\mathbf{R}}\right).$$

In this scenario, the observed data, D, are not the individual-level genotypes and phenotypes ($\mathbf{X}$, $\mathbf{y}$), but rather D = ($\widehat{\boldsymbol{\beta}}_{\mathrm{GWAS}}$, $\widehat{\mathbf{R}}$), where $\widehat{\mathbf{R}}$ is an estimate of LD computed from either the genotypes of a set of individuals in the GWAS ("in-sample" LD) or from an external reference panel (e.g., 1000 Genomes[57]). By combining the prior on $\boldsymbol{\beta}$, $p(\boldsymbol{\beta}|\boldsymbol{\lambda})$ ($\boldsymbol{\lambda}$ represents the hyperparameters of the prior over $\boldsymbol{\beta}$), and the likelihood of the observed data, $p(\widehat{\boldsymbol{\beta}}_{\mathrm{GWAS}}|\boldsymbol{\beta}, \widehat{\mathbf{R}}, \sigma_e^2)$, one can compute the posterior distribution of the causal effects, $p(\boldsymbol{\beta}|\widehat{\boldsymbol{\beta}}_{\mathrm{GWAS}}, \widehat{\mathbf{R}}, \boldsymbol{\lambda}, \sigma_e^2)$. The hyperparameters, $\boldsymbol{\lambda}$ and σ_e^2, can be estimated via empirical Bayes (e.g., as implemented in SuSiE[42]).

The posterior of $\boldsymbol{\beta}$, $p(\boldsymbol{\beta}|\mathrm{D})$, is, in general, computationally intractable. However, approximate inference, e.g., Markov chain Monte Carlo (MCMC) or variational inference, can be used to approximate the posterior as $\tilde{p}(\boldsymbol{\beta}|\mathrm{D})$. In this work, we use SuSiE,[42] a variational inference-based implementation of linear regression that assumes a sparse prior, but in principle, it is straightforward to use any implementation of linear regression with a sparse prior. We draw P samples from the posterior of the causal effects, $\tilde{\boldsymbol{\beta}}^{(1)}, \ldots, \tilde{\boldsymbol{\beta}}^{(P)} \sim p(\boldsymbol{\beta}|\mathrm{D})$, and use these posterior samples to approximate the full posterior distribution of h_{gene}^2, i.e., $(\tilde{\boldsymbol{\beta}}_g^{(1)})^{\mathrm{T}}\widehat{\mathbf{R}}_g(\tilde{\boldsymbol{\beta}}_g^{(1)}), \ldots, (\tilde{\boldsymbol{\beta}}_g^{(P)})^{\mathrm{T}}\widehat{\mathbf{R}}_g(\tilde{\boldsymbol{\beta}}_g^{(P)})$. Given the approximate posterior of h_{gene}^2, one can compute any summary statistic of interest. Here, we report the estimated posterior mean,

$$\widehat{h}_{\mathrm{gene}}^2 = \widehat{\mathrm{E}}\left[\boldsymbol{\beta}_g^{\mathrm{T}}\mathbf{R}_g\boldsymbol{\beta}_g\middle|\mathrm{D}\right] = \frac{1}{P}\sum_{p=1}^{P}\left(\tilde{\boldsymbol{\beta}}_g^{(p)}\right)^{\mathrm{T}}\widehat{\mathbf{R}}_g\left(\tilde{\boldsymbol{\beta}}_g^{(p)}\right),$$

and credible intervals, which are one possible metric of uncertainty (described below). The same procedure can be used to estimate the component of gene-level heritability explained by a subset of the SNPs assigned to the gene (such as a MAF-based annotation).

For computational efficiency, we partition the genome into approximately independent LD blocks[58] and approximate the posterior distribution of $\boldsymbol{\beta}$ separately for each LD block; the approximate independence of each LD block from the rest of the genome implies that the causal effects at SNPs outside of the LD block of interest are absorbed into the environmental noise term. Similarly, the hyperparameters $(\boldsymbol{\lambda}, \sigma_e^2)$ are specific to and estimated independently for each LD block.

Quantifying uncertainty in gene-level heritability estimates

The posterior samples $\tilde{\boldsymbol{\beta}}^{(1)}, \ldots, \tilde{\boldsymbol{\beta}}^{(P)}$ provide an approximation to the full posterior distribution of $\boldsymbol{\beta}$, thus capturing uncertainty in the causal effect sizes arising from two main sources: LD and finite GWAS sample size (Figure 1). By using the full posterior of $\boldsymbol{\beta}$ to approximate the full posterior of h_{gene}^2, we propagate the uncertainty in the causal effects into our estimate of h_{gene}^2. (The noise in $\widehat{\mathbf{R}}$ is also an important factor, but for simplicity, we investigate uncertainty in $\widehat{h}_{\mathrm{gene}}^2$ in simulations where $\widehat{\mathbf{R}} = \mathbf{R}$.)

We summarize the uncertainty in $\widehat{h}_{\mathrm{gene}}^2$ by computing ρ-level credible intervals (ρ-CIs). For a given $\rho \in [0, 1]$, ρ-CI is defined as

the central interval within which h^2_{gene} lies with probability ρ. In other words, the upper and lower bounds of ρ-CI are set to the empirical $(1-\rho)/2$ and $1-(1-\rho)/2$ quantiles of the posterior samples $(\tilde{\boldsymbol{\beta}}_g^{(p)})^{\mathrm{T}}\widehat{\mathbf{R}}_g(\tilde{\boldsymbol{\beta}}_g^{(p)}), p = 1,\ldots,P$.

Implementation details

We partition the genome into approximately independent LD blocks[58] and, for each gene of interest, we perform inference on the LD block containing the gene. For each LD block, we extract the marginal association statistics and estimate LD for all the variants in the LD block. We estimate the posterior distribution of effect sizes by using the function "susie_suff_stat" with default parameters, as implemented in SuSiE[42] v0.8 (web resources). We use the function "susie_get_posterior_samples" to obtain 500 posterior samples.

Simulation framework

We simulate phenotypes from the real imputed genotypes of N = 290,273 "unrelated White British" individuals in the UK Biobank, obtained by extracting individuals with self-reported British ancestry who are greater than third-degree relatives (pairs of individuals with kinship coefficient $< 1/2^{(9/2)}$, as defined in Bycroft et al.[47]). Filtering on MAF > 0.5% leaves M = 200,235 variants on chromosome 1 from which to draw phenotypes.

The genotypes of the above individuals can be encoded as $g_{ni} \in \{0,1,2\}$, the number of copies of the effect allele carried by individual n at variant i, for all $n = 1,\ldots,N$ and $i = 1,\ldots,M$. We assume that the population and in-sample allele frequencies are the same, and we standardize the genotype vector at each variant to have mean 0 and variance 1 across individuals by computing $x_{ni} = (g_{ni} - 2f_i)/\sqrt{2f_i(1-f_i)}$. Importantly, this genotype standardization is equivalent to assuming that the variance of the *per-allele* causal effect at variant i is proportional to $[f_i(1-f_i)]^{-1}$ — a relatively strong inverse coupling between allele frequency and allelic effect size.[59]

Given the standardized genotypes, we simulated phenotypes under a variety of genetic architectures by varying the number of causal genes and background polygenicity, p_{causal}. Total SNP heritability on chromosome 1 was fixed to $h^2_G = 0.05$ and cumulative gene-level heritability was fixed to $\sum_k h^2_{\text{gene},k} = 0.03$. First, we uniformly sample 3%, 8%, or 16% of the 1,083 genes on chromosome 1 (web resources) to be causal ($h^2_{\text{gene},k} > 0$). Second, for each causal gene, we draw causal variants uniformly from the set of variants in the gene body and within 10 kb upstream/downstream of the gene start/end positions; the causal variants in the window around the gene are intended to represent regulatory causal variants in transcription start sites (TSSs). The causal configuration is set to either (1) five causal variants in the gene body and three causal variants in TSS or (2) ten causal variants in the gene body and six causal variants in TSS. Third, for each variant not considered in the previous step (i.e., the variants that are not located within 10 kb upstream/downstream of any gene's start/end positions), we draw its causal status as $c_i \sim Bernoulli(p_{\text{causal}})$ for $p_{\text{causal}} = \{0.001, 0.01\}$.

Finally, for the variants with $c_i = 1$, we draw independent standardized causal effect sizes as $\beta_i \sim N(0,\sigma_i^2)$, assuming $cov(\beta_i,\beta_j) = 0$ for all $i \neq j$. β_i is set to 0 if $c_i = 0$. The value of σ_i^2 is determined by whether the causal variant is located in a gene body, in a TSS, or elsewhere. Let b, t, and q represent the total number of causal variants in gene bodies, TSSs, and the background, respectively. We assume that causal variants in gene bodies explain the same amount of cumulative gene-level heritability; thus, these variants have $\sigma_i^2 = (1/b)\sum_k h^2_{\text{gene},k} = 0.03/b$. Similarly, we assume that all causal variants in TSSs together have a heritability of 0.01, which corresponds to $\sigma_i^2 = 0.01/t$ for these variants. The remaining 0.01 heritability is also assumed to be distributed evenly across the background causal variants, so these variants have $\sigma_i^2 = 0.01/q$. We note that the causal statuses and effect sizes for each variant are only drawn once; the environmental noise term is drawn 30 times independently to generate 30 simulation replicates.

Again, we emphasize that even though the *standardized* causal effects in gene bodies are drawn *i.i.d.* from $\beta_i \sim N\left(0, \frac{0.03}{b}\right)$ regardless of allele frequency, the assumption of an inverse relationship between *per-allele* causal effects and allele frequency has already been baked into the simulation framework through the initial genotype standardization.

Evaluating and comparing gene-level heritability estimates in simulations

Recall that for a given gene g, the causal effect sizes and LD of the variants assigned to the gene are denoted $\boldsymbol{\beta}_g$ and $\mathbf{R}_g$, and ground-truth gene-level heritability is defined as $h^2_{\text{gene}} = \mathrm{E}_{\boldsymbol{\beta}}[\boldsymbol{\beta}_g^{\mathrm{T}}\mathbf{R}_g\boldsymbol{\beta}_g]$. The posterior mean estimated for a single simulation replicate s is denoted $\widehat{h}^2_{\text{gene},(s)}$. We estimate the bias of the estimator as $\mathrm{bias}\left(\widehat{h}^2_{\text{gene}}\right) \approx \frac{1}{30}\sum_s\left(\widehat{h}^2_{\text{gene},(s)} - h^2_{\text{gene}}\right)$; the variance of the estimator as $\mathrm{Var}\left[\widehat{h}^2_{\text{gene}}\right] \approx \frac{1}{30}\sum_s\left(\widehat{h}^2_{\text{gene},(s)} - h^2_{\text{gene}}\right)^2$; and the mean squared error as $\mathrm{MSE}[\widehat{h}^2_{\text{gene}}] = (\mathrm{bias}[\widehat{h}^2_{\text{gene}}])^2 + \mathrm{Var}[\widehat{h}^2_{\text{gene}}]$.

For each simulation replicate s, we output ρ-level credible intervals, defined as

$$\mathrm{CI}(\rho,s) = \left(\widehat{h}^2_{\text{gene},\frac{1-\rho}{2},(s)},\ \widehat{h}^2_{\text{gene},1-\frac{1-\rho}{2},(s)}\right)$$

where the $(1-\rho)/2$ and $1-(1-\rho)/2$ percentiles are estimated from $P = 500$ posterior samples; we use $\rho = 0.9$ instead of 0.95 to obtain more robust credible intervals from 500 posterior samples. To assess the accuracy of credible intervals, we calculate "empirical coverage" across simulation replicates, defined as the proportion of simulation replicates in which the ρ-level credible interval covers the ground-truth gene-level heritability: $(1/30)\sum_s \mathbb{I}[\widehat{h}^2_{\text{gene},(s)} \in \mathrm{CI}(\rho,s)]$.

Estimating the number of nonzero-heritability genes

We explore two metrics for quantifying polygenicity at the gene level that do not use 90%-CIs. First, for the k-th gene, we estimate the posterior probability that $h^2_{\text{gene},k} > 0$ from $p = 1,\ldots,500$ posterior samples as

$$p\left(h^2_{\text{gene},k} > 0 \middle| \mathrm{D}\right) \approx \frac{1}{500}\sum_{p=1}^{500}\mathbb{I}\left[\left(\tilde{\boldsymbol{\beta}}_{g,k}^{(p)}\right)^{\mathrm{T}}\widehat{\mathbf{R}}_{g,k}\left(\tilde{\boldsymbol{\beta}}_{g,k}^{(p)}\right) > 0\right]$$

where $\mathbb{I}$ is an indicator function that evaluates to 1 if $(\tilde{\boldsymbol{\beta}}_{g,k}^{(p)})^{\mathrm{T}}\widehat{\mathbf{R}}_{g,k}(\tilde{\boldsymbol{\beta}}_{g,k}^{(p)}) > 0$ and to 0 otherwise. The total number of nonzero-heritability genes is then estimated by summing the posterior probabilities across genes:

$$\frac{1}{500}\sum_{k}\sum_{p=1}^{500}\mathbb{I}\left[\left(\tilde{\boldsymbol{\beta}}_{g,k}^{(p)}\right)^{\mathrm{T}}\widehat{\mathbf{R}}_{g,k}\left(\tilde{\boldsymbol{\beta}}_{g,k}^{(p)}\right)>0\right].$$

The second quantity we estimate is the number of genes that explain 50% of the cumulative gene-level heritability. This is done by rank ordering genes by their estimated posterior means, $\widehat{h}^2_{\mathrm{gene},k}$, and summing the posterior means across genes, starting with the largest estimate, until $\geq(1/2)\sum_k \widehat{h}^2_{\mathrm{gene},k}$ is reached.

Comparison to "naïve" gene-level heritability estimator

We compare our approach to an alternative "naïve" estimator of gene-level heritability that does not model LD between the gene and its adjacent regions and thus ignores causal-effect uncertainty. This estimator is similar to existing methods that are meant to be applied to approximately independent LD blocks.[34,60] For each gene, we extract the marginal association statistics, $\widehat{\boldsymbol{\beta}}_g$, and the estimated LD, $\widehat{\mathbf{R}}_g$, for the variants assigned to the gene, and we compute the alternative estimator as $\left(N\widehat{\boldsymbol{\beta}}_g^{\top}\widehat{\mathbf{R}}_g^{\dagger}\widehat{\boldsymbol{\beta}}_g-q\right)\Big/(N-q)$, where $\widehat{\mathbf{R}}_g^{\dagger}$ and q are the pseudo-inverse and rank of $\widehat{\mathbf{R}}_g$, respectively.[34,60]

Assessing robustness to LD panel sample size

To assess the robustness of our approach to the sample size of the LD panel used to estimate LD, we randomly draw a subset of N = {500, 1,000, 2,500, 5,000} individuals from the full 290,273 individuals. After extracting variants with MAF > 0.5%, genotypes are standardized to have mean 0 and variance 1, similar to the full-sample analysis. Because we are interested in assessing robustness to noisy estimates of LD, all analyses are performed with the same set of marginal association statistics used in the full-sample analysis, excluding the variants that were filtered from the LD panel based on MAF. The LD and marginal association statistics are fed into the "h2gene" software, similar to the full-sample analysis.

Analysis of 25 UK Biobank phenotypes

We analyzed 25 quantitative phenotypes in the self-reported "White British" cohort in the UK Biobank (web resources). Phenotypes and imputed genotypes were filtered according to the same procedures used in the simulation analyses, leaving N = 290,273 individuals and M = 5,650,812 variants with MAF > 0.5%. Quantitative phenotypes were quantile-normalized to a Gaussian distribution with mean 0 and variance 1. We then performed a GWAS for each trait using the "–assoc" option in PLINK (web resources) with age, sex, and the top ten genetic principal components (PCs) included as covariates. The genetic PCs were precomputed by the UK Biobank via fastPCA[61] applied to genotypes measured at 147,606 SNPs (MAF > 1%) in 407,599 "unrelated" individuals.[47]

In-sample LD was computed for each approximately independent LD block.[58] We downloaded gene names and coordinates (web resources) and, for each gene, we define the estimand of interest to be a function of the variants in the gene body *and* those located within 10 kb upstream/downstream of the gene start/end positions. Finally, given the in-sample LD and marginal association statistics, we infer the posterior distribution of the causal effect sizes one LD block at a time, and we estimate and partition gene-level heritability for all genes in each LD block, where we define the estimand of interest to be a function of the variants in the gene body *and* those located within 10 kb upstream/downstream of the gene start/end positions. MAGMA v1.09 was used for gene-level association testing with a 10-kb window around each gene. The same list of genes and the same set of imputed variants were used for the MAGMA analysis.

Additional quality control to mitigate rare-variant population stratification

Including the top 10–20 genome-wide PCs as covariates in a GWAS is a standard approach to controlling for population structure. However, because the PCs included in the UK Biobank data release were computed from common SNPs (MAF > 1%), our GWASs may be susceptible to false positives driven by population stratification among rare variants, which can exhibit stratification patterns quite different from those of common variants.[62,63] If there is population structure of recent origin *and* the confounding environmental effects are smoothly distributed with respect to ancestry, PCs computed from rare variants may be able to correct for confounding resulting from this recent structure.[64] However, because the distribution of confounding environmental effects is unknown *a priori*, we cannot tell whether a rare-variant PC correction would be sufficient for this analysis. Ideally, we would perform PCA on rare variants (MAF < 1%) and include the top PCs as covariates in the GWASs anyway, but this would require whole-genome sequencing data from the "unrelated White British" UK Biobank cohort, which are not readily available to us at this time.

While single rare-variant association tests are prone to false positives resulting from uncorrected recent and/or local population structure, aggregating evidence from multiple rare variants can make an association statistic more robust to such structure. This is because adding more rare variants to a single test statistic increases the recombination distance between the variants included in the test. Therefore, to try to reduce potential false positives from rare-variant stratification in the real-data analyses, we exclude genes in the bottom 5$^{\mathrm{th}}$ percentile in terms of (1) the number of rare variants in the gene body ± 10 kb, which in this case corresponds to genes with <4 rare variants (Figure S19A), or (2) [number of rare variants in the gene body ± 10 kb] / [gene length], which in this case is <0.00021 (Figure S19B). This reduces the original set of 17,437 protein-coding genes to 15,770.

Results

Overview of the method

Given an assignment of m_g variants to a gene of interest, total gene-level heritability is defined as $h^2_{\mathrm{gene,t}}\equiv\mathrm{Var}[\mathbf{x}_g^T\boldsymbol{\beta}_g|\boldsymbol{\beta}]=\mathbb{E}_{\boldsymbol{\beta}}[\boldsymbol{\beta}_g^{\mathrm{T}}\mathbf{R}_g\boldsymbol{\beta}_g]$, where $\boldsymbol{\beta}_g$ is the $m_g\times1$ vector of unknown causal effect sizes and $\mathbf{R}_g$ is the $m_g\times m_g$ LD for SNPs in the gene (material and methods). Our goal in this work is to estimate a "distribution" over $h^2_{\mathrm{gene,t}}$ that captures uncertainty in the causal effects that arises from LD and finite GWAS sample size (Figure 1A).

To this end, we adopt a probabilistic fine-mapping framework[35,42] that assumes a sparse prior on the causal effect sizes in the LD block containing the gene and infers the posterior distribution of the causal effect sizes, $p(\boldsymbol{\beta}|\widehat{\boldsymbol{\beta}},\widehat{\mathbf{R}})$, where $\widehat{\boldsymbol{\beta}}$ is the vector of estimated marginal effects from GWAS and $\widehat{\mathbf{R}}$ is an estimate of LD. By sampling from the posterior of $\boldsymbol{\beta}$, we generate an approximation to

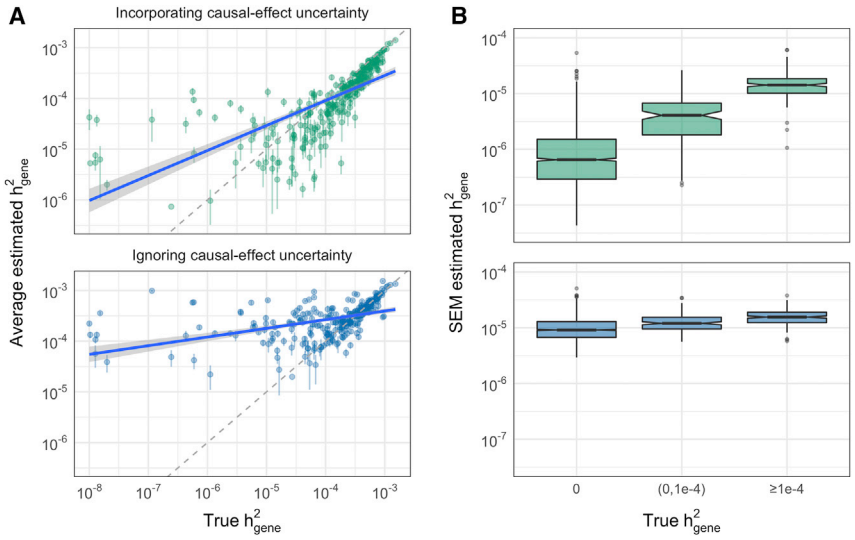

Figure 2. Impact of causal-effect uncertainty on gene-level heritability estimation in simulations

Chromosome 1, MAF > 0.5%, $p_{causal} = 0.01$, N = 290K individuals, and 1,038 genes, of which 16% have nonzero gene-level heritability.

(A) Average posterior mean of $h^2_{gene,t}$ ($\pm 1.96 \times$ SEM) (green) and average "naive" estimate (blue) for a given gene across 30 simulation replicates. To facilitate visualization, only genes with $h^2 > 10^{-8}$ are shown.

(B) SEM of $\widehat{h}^2_{gene,t}$ (green) and of the naive estimator (blue) with respect to the underlying value of $h^2_{gene,t}$.

the posterior of $h^2_{gene,t}$ (Figure 1B, material and methods). For each gene, we report the estimated posterior mean ($\widehat{h}^2_{gene,t}$) and ρ-level credible interval (ρ-CI), defined as the central interval that contains the true gene-level heritability with probability ρ. Whereas previous works applied similar approaches to generate credible sets of causal variants[42] or to estimate regional SNP-heritability of LD blocks,[35] our goal in this work is to estimate the heritability explained by any arbitrary (not necessarily contiguous) set of variants much smaller than an LD block.

Using the same approach, we estimate the components of gene-level heritability attributable to the rare ($0.5\% \leq$ MAF $< 1\%$), low-frequency ($1\% \leq$ MAF $< 5\%$), and common (MAF $\geq 5\%$) variants assigned to the gene of interest; we denote these quantities $h^2_{gene,r}$, $h^2_{gene,lf}$, and $h^2_{gene,c}$, respectively (material and methods). (We note that, while there are many definitions of "rare" in the literature, we threshold at MAF $\geq$ 0.5% to reduce potential noise from imputation; see discussion for details.)

Accuracy of gene-level heritability estimates in simulations

We perform simulations starting from real imputed genotypes of N = 290,273 "unrelated White British" individuals in the UK Biobank (chromosome 1, MAF > 0.5%, M = 200,235 variants, 1,083 genes; material and methods). In all simulations, the estimand of interest (gene-level heritability, $h^2_{gene,t}$) is the proportion of phenotypic variance explained by the variants in the gene body. We note that our choice of variant assignment is arbitrary; there are many ways to assign variants to a gene, but our goal in this section is to provide a proof of concept. In brief, our simulation framework consists of three steps. First, for a given total heritability (variance explained by all M variants) and cumulative gene-level heritability (variance explained by all genes), we randomly select 3%, 8%, or 16% of the genes to have $h^2_{gene,t} > 0$. Second, for each gene with $h^2_{gene,t} > 0$, we draw causal variants in the gene body and within 10 kb upstream/downstream of the gene start/end positions; the purpose of the latter is to create situations where the estimated effects of variants in the region of interest are inflated in part because they tag causal variants located adjacent to the region. Third, we sample noncoding "background" causal variants from the rest of the chromosome with frequency $p_{causal} = \{0.001, 0.01\}$. Under this model, the majority of simulated gene-level heritabilities are on the order of 10^{-6} to 10^{-3} (Figure S1), similar to what we observe in real data in subsequent sections (e.g., Figure S20).

For each gene, we compute two metrics of accuracy from 30 simulation replicates: bias$[\widehat{h}^2_{gene,t}]$ and MSE$[\widehat{h}^2_{gene,t}]$ (mean squared error) (material and methods). Overall, the estimated posterior means ($\widehat{h}^2_{gene,t}$) are concordant with the true values of $h^2_{gene,t}$ (Figure 2, Figure S2). For example, among just the causal genes ($h^2_{gene,t} > 0$) in the "most polygenic" simulations (where 16% of genes have nonzero heritability and per-causal-variant effect sizes are smallest), the estimator is slightly downward-biased for values $> 10^{-4}$ and upward-biased for smaller value, but generally within the correct order of magnitude (Figure 2). To illustrate the impact of causal-effect uncertainty on gene-level heritability estimation, we compare $\widehat{h}^2_{gene,t}$ to a naive estimator that ignores LD between the gene and its adjacent regions, thus ignoring causal-effect uncertainty (material and methods). As expected, the naive estimator is significantly more inflated (Figure 2); in particular, many zero-heritability genes have dramatically upward-biased estimates (Figure S3) due to LD between variants in the gene and nearby causal variants. As expected, MSE$[\widehat{h}^2_{gene,t}]$ increases with p_{causal}, the proportion of causal genes, and gene length (Figures S4–S6); average LD score and average MAF of variants in the gene have no discernible impact (Figures S5, S7, and S8).

We also benchmark the estimators for $h^2_{gene,c}$, $h^2_{gene,lf}$, and $h^2_{gene,r}$. Unlike $\widehat{h}^2_{gene,t}$, $\widehat{h}^2_{gene,c}$ and $\widehat{h}^2_{gene,lf}$, which display upward bias for values $< 10^{-4}$, $\widehat{h}^2_{gene,r}$ is slightly downward-biased across all values of h^2 (Figure 3). As with $\widehat{h}^2_{gene,t}$, MSE$[\widehat{h}^2_{gene,r}]$ increases with $h^2_{gene,r}$, p_{causal}, the proportion of causal genes, and gene length (Figures S4–S6) and

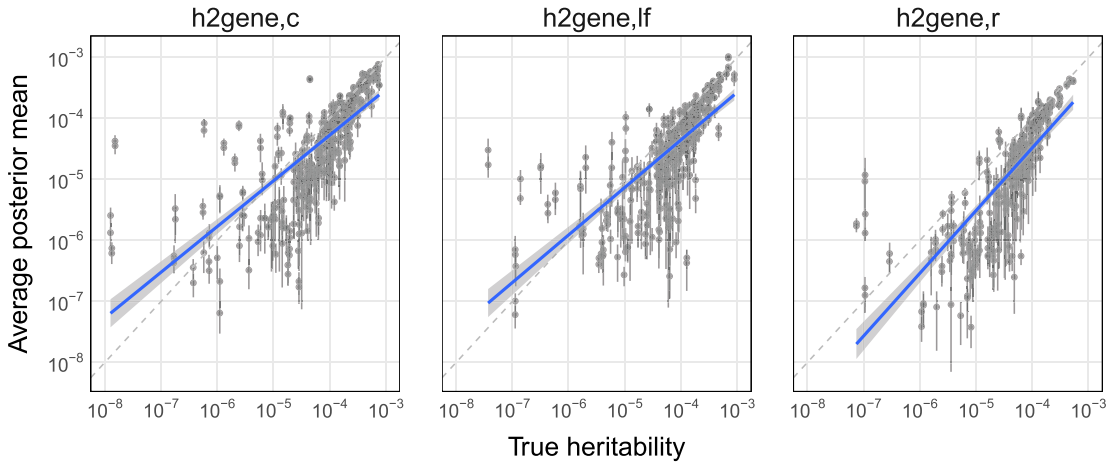

Figure 3. Estimates of h^2 contributions from common, low-frequency, and rare variants in simulations
Simulations were performed on chromosome 1 variants (MAF > 0.5%), with $p_{causal} = 0.01$, N = 290K individuals, and 1,083 genes, of which 16% have nonzero heritability. To facilitate visualization, and because all estimates in real traits were greater than 10^{-8}, only genes with $h^2 > 10^{-8}$ are shown. Each point is the average posterior mean for one gene across 30 simulation replicates; error bars mark ± 1.96 x SEM.

does not noticeably vary with respect to average LD score or average MAF of variants in the gene (Figures S5, S7, and S8).

Calibration of ρ-credible intervals (ρ-CIs)

Recall that ρ-CI is defined as the central interval containing the true gene-level heritability with probability $\rho \in [0, 1]$. We assessed calibration of ρ-CIs by using "empirical coverage," the proportion of simulation replicates in which ρ-CI contains the true gene-level heritability (material and methods). Perfect calibration of ρ-CI would manifest as empirical coverage equal to ρ for all $\rho \in [0, 1]$. In reality, we observe a downward bias in empirical coverage across all simulations that increases in magnitude as the proportion of causal genes increases (i.e., as per-variant causal effect sizes decrease); for example, at $\rho = 0.9$, empirical coverage ranges from approximately 0.75 when 3% of genes are causal to 0.65 when 16% are causal (Figure S9). While downward bias in empirical coverage could result from ρ-CIs underestimating or overestimating $h^2_{gene,t}$, we find that, for true nonzero-heritability genes, the credible intervals at $\rho = \{0.90, 0.95\}$ tend to underestimate $h^2_{gene,t}$. For example, at $\rho = 0.95$, as polygenicity increases from 3% to 16%, the average (and standard error of the mean [SEM]) proportion of genes with $h^2_{gene,t} > 0$ that are underestimated increases from approximately 14% (0.7%) to 29% (0.7%) while the average overestimated decreases from 6% (0.4%) to 3.5% (1.5%), respectively. The ρ-CIs for $h^2_{gene,r}$ are more conservative; for the same parameters, the proportion of $h^2_{gene,r} > 0$ genes that are underestimated increases from 38% (1%) to 45% (0.6%) while the proportion overestimated decreases from 1.5% (0.3%) to 0.7% (0.1%) (Table S2, Figure S10).

We estimate the power of ρ-CI at $\rho = 0.9$ as the proportion of nonzero-h^2 genes correctly identified at the significance threshold 90%-CI > 0. As expected, power is higher in simulations where the average values of $h^2_{gene,t}$ and $h^2_{gene,r}$ are larger (i.e., when polygenicity is lower) and is higher overall for $h^2_{gene,t}$ than for $h^2_{gene,r}$ (Figure 4A). We also assess power with respect to the underlying value of $h^2_{gene,t}$ or $h^2_{gene,r}$, estimated for each nonzero-h^2 gene as the proportion of simulation replicates in which the gene correctly passes the threshold 90%-CI > 0. In the most polygenic simulations, power ranges from an average of 56% for genes in the lowest $h^2_{gene,t}$ quartile ($h^2_{gene,t} < 2 \times 10^{-5}$) to 94% for the highest quartile ($h^2_{gene,t} > 4 \times 10^{-4}$) (Figure S11A). For $h^2_{gene,r}$, power is significantly lower, ranging from an average of 10% for genes with $h^2_{gene,r}$ in the lower 50th percentile ($h^2_{gene,r} < 3 \times 10^{-5}$) to 72% for genes in the highest quartile ($h^2_{gene,r} > 8 \times 10^{-5}$) (Figure S11B).

Since we are interested in using 90%-CIs to identify narrow sets of high-impact genes, it is also useful to assess the false positive rate (FPR) and positive predictive value (PPV). We estimate FPR as the proportion of zero-heritability genes that incorrectly pass the threshold 90%-CI > 0. For $h^2_{gene,t}$, FPR ranges from approximately 19% (SEM 0.2%) when 3% of genes are causal to 21% (0.2%) when 16% of genes are causal (Figure S12A). FPR is overall much smaller for $h^2_{gene,r}$ and decreases as polygenicity increases, ranging from 0.2% (0.01%) when 16% of genes are causal to 0.5% (0.01%) when 3% of genes are causal (Figure S12B). Although the FPR for $h^2_{gene,t}$ is relatively high, most genes passing the 90%-CI > 0 threshold that have $\widehat{h^2}_{gene,t} > 10^{-4}$ are true positives (Figure S12C).

We estimate PPV as the proportion of genes with 90%-CI > 0 that are, in fact, true positives. Despite its relatively low power, $h^2_{gene,r}$ 90%-CI > 0 has a dramatically higher PPV than does $h^2_{gene,t}$ 90%-CI > 0 (Figure 4B). PPV increases as polygenicity increases (i.e., as causal effect sizes decrease), reaching an average of 35% (SEM 0.2%) for $h^2_{gene,t}$ and 88% (0.5%) for $h^2_{gene,r}$. That is, in simulations where 16% of genes are causal, approximately 88% of genes identified at the

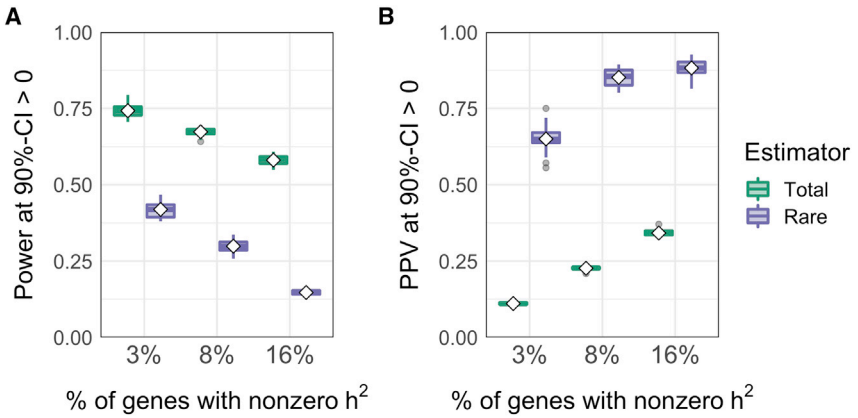

Figure 4. Power and PPV at 90%-CI > 0 in simulations

(A) Power is estimated per simulation replicate as the proportion of nonzero-h^2 genes correctly identified at $h^2_{\text{gene,t}}$ 90%-CI > 0 (green) or $h^2_{\text{gene,r}}$ 90%-CI > 0 - (purple).

(B) PPV is estimated per simulation replicate as the proportion of genes identified at 90%-CI > 0 that are, in fact, true positives. Each boxplot represents 30 simulation replicates; white diamonds mark the mean.

significance threshold $h^2_{\text{gene,r}}$ 90%-CI > 0 have $h^2_{\text{gene,r}} > 0$, while only 35% of the genes identified at $h^2_{\text{gene,t}}$ 90%-CI > 0 have $h^2_{\text{gene,t}} > 0$. Moreover, the genes identified at $h^2_{\text{gene,r}}$ 90%-CI > 0 are enriched for genes with ≥50% of $h^2_{\text{gene,t}}$ attributable to $h^2_{\text{gene,r}}$. In the same simulations, genes with $h^2_{\text{gene,r}}/h^2_{\text{gene,t}} > 0.5$ comprise 24% of all genes with $h^2_{\text{gene,r}} > 0$ and 14% of all genes with $h^2_{\text{gene,t}} > 0$; PPV for identifying these genes at 90%-CI > 0 is 39% for $h^2_{\text{gene,r}}$ and 4% for $h^2_{\text{gene,t}}$ (Figure S13). In other words, approximately 39% of genes with $h^2_{\text{gene,r}}$ 90%-CI > 0 have ≥50% of $h^2_{\text{gene,t}}$ explained by rare causal variants, whereas only 4% of genes with $h^2_{\text{gene,t}}$ 90%-CI > 0 fall in this category. This corresponds to a 1.6× enrichment of genes with $h^2_{\text{gene,r}}/h^2_{\text{gene,t}} > 0.5$ among those identified at the threshold $h^2_{\text{gene,r}}$ 90%-CI > 0 and a depletion of these genes at $h^2_{\text{gene,t}}$ 90%-CI > 0.

Quantification of polygenicity and related quantities in simulations

We explore different approaches for estimating the total number of nonzero-h^2 genes. First, we estimate the expected number of nonzero-h^2 genes by approximating, for each gene, the posterior probability that $h^2_{\text{gene,t}} > 0$ and summing the posterior probabilities across genes (material and methods). Unsurprisingly, because the method is not calibrated to be applied in this way, this approach produces highly inflated estimates (Figure S14A). The number of genes with 90%-CI > 0 is also a biased estimator; in lower-polygenicity settings (larger per-gene heritabilities), it overestimates the number of nonzero-h^2 genes for both $h^2_{\text{gene,t}}$ and $h^2_{\text{gene,c}}$, and in higher-polygenicity settings (smaller per-gene heritabilities), it underestimates for $h^2_{\text{gene,lf}}$ and $h^2_{\text{gene,r}}$ (Figure S14B). However, across all simulation settings, we found that we obtain nearly unbiased estimates of the number of genes explaining 50% of the cumulative gene-level heritability by (1) rank ordering genes by $\widehat{h}^2_{\text{gene}}$ and (2) summing $\widehat{h}^2_{\text{gene}}$ across genes, from largest to smallest, until $\geq 0.5\sum_k \widehat{h}^2_{\text{gene}_k}$ is reached (Figure S15). This metric captures the concentration or dispersion of heritability across genes—an important aspect of genetic architecture. Note that the estimated cumulative gene-level heritability, $\sum_k \widehat{h}^2_{\text{gene}_k}$, is a sum across all genes, not just those that pass 90%-CI > 0. That we can accurately estimate the number of genes explaining $\geq 0.5\sum_k \widehat{h}^2_{\text{gene}_k}$ is consistent with the trends we observe in bias$[\widehat{h}^2_{\text{gene,t}}]$ (Figure 2A), i.e., the slight downward bias we observe in $\widehat{h}^2_{\text{gene,t}}$ for larger values (e.g., $h^2_{\text{gene,t}} \geq 10^{-5}$) and the upward bias we observe for smaller values (e.g., $h^2_{\text{gene,t}} < 10^{-5}$).

Robustness to noise in estimates of LD

Finally, we assess whether $\widehat{h}^2_{\text{gene,t}}$ is robust to the number of individuals used to estimate LD, i.e., the sample size of the "LD panel" (material and methods). Compared to in-sample LD computed from the full set of individuals in the GWAS (N = 290,273), using a random subset of N = {500, 1,000, 2,500, 5,000} individuals from the original GWAS does not significantly impact the MSE of $\widehat{h}^2_{\text{gene,t}}$ or $\widehat{h}^2_{\text{gene,r}}$ (Figure S16). Using 90%-CIs to identify nonzero-h^2 genes, we find that the FPR (the proportion of zero-heritability genes incorrectly identified at 90%-CI > 0) is robust with respect to LD panel sample size for both $h^2_{\text{gene,t}}$ and $h^2_{\text{gene,r}}$ (Figure S17). Power (the proportion of true nonzero-h^2 genes identified at 90%-CI > 0) is relatively robust to LD panel sample size in the most polygenic setting; however, in the least polygenic setting, power drops more significantly, from ~73% at the full sample size to ~47% at N = 500 (Figure S18A). We observe a similar drop in power for $h^2_{\text{gene,r}}$ (Figure S18B). Thus, while using a smaller sample of individuals from the GWAS cohort does not significantly increase type I error, we recommend using the full GWAS cohort to compute in-sample LD in order to maximize power, especially for $h^2_{\text{gene,r}}$.

Gene-level heritability estimates for 25 quantitative traits in the UK Biobank

We estimate, and partition by MAF, the gene-level heritabilities of 15,770 protein-coding genes for 25 well-powered quantitative traits in the UK Biobank (N = 290,273

Table 1. Summary of h^2_{gene} estimates across 25 quantitative traits (N = 290K "White British," UK Biobank)

Trait	Num. genes w/ $h^2_{gene,t}$ 90%-CI > 0	Num. genes that explain $\geq 0.5 \sum \hat{h}^2_{gene,t}$	$h^2_{gene,t} = h^2_{gene,c}$	$h^2_{gene,t} = h^2_{gene,lf}$	$h^2_{gene,t} = h^2_{gene,r}$
Alkaline phosphatase	1,542	21	1,142	108	18
Apolipoprotein A-I	1,589	71	1,186	105	11
Basal metabolic rate	1,929	568	1,476	115	10
BMD heel T-score	1,297	251	1,006	76	3
BMI	1,722	677	1,312	98	6
C-reactive protein	1,561	9	1,187	88	6
Corneal hysteresis	1,103	321	833	74	3
Cystatin C	1,738	163	1,328	110	8
Forced vital capacity	1,748	565	1,337	108	5
GGT	1,650	166	1,256	101	12
Hair color	1,201	7	883	77	13
HbA1c	1,676	116	1,240	133	17
HDL	1,602	59	1,194	109	11
Height	2,258	445	1,713	152	27
High light scatter reticulocyte count	1,696	188	1,279	112	23
IGF-1	1,691	270	1,265	116	10
MCH	1,557	109	1,151	122	15
MSCV	1,585	144	1,226	101	8
Monocyte count	1,601	144	1,219	100	9
Mean platelet volume	1,753	57	1,291	127	25
Platelet count	1,748	158	1,351	102	24
Platelet distrib. width	1,598	44	1,219	102	16
RBC count	1,752	310	1,341	122	18
SHBG	1,551	7	1,164	102	17
Urate	1,584	38	1,206	103	12

Column 2: number of genes (out of 15,770) with (1) $h^2_{gene,t}$ 90%-CI > 0 and (2) 90%-CI > 0 for at least one MAF bin (rare, low-frequency, or common). Column 3: estimated number of genes that explain 50% of cumulative $h^2_{gene,t}$. Columns 4–6: numbers of 90%-CI > 0 genes with effects exclusively from common, low-frequency, or rare variants. (BMD, bone mineral density; MCH, mean corpuscular hemoglobin; MSCV, mean sphered corpuscular volume; RBC, red blood cell.)

"unrelated White British" individuals,[47] M = 5,650,812 with MAF > 0.5%, imputed data; material and methods). These 25 traits are a mix of serum and urine biomarker traits (many of which have known "causal" genes and biochemical pathways[65–68]) and highly polygenic anthropometric traits (Table 1). Because our GWASs may contain uncorrected fine-scale population structure among rare variants (discussion), to reduce potential false positives, we exclude genes in the bottom 5th percentile in terms of (1) number of rare variants or (2) number of rare variants divided by gene length (Figure S19, material and methods). Unless otherwise stated, the estimands of interest are functions of the variants located in the gene body *and* the variants located within 10 kb upstream/downstream of the gene start/end positions. A gene is classified as having "nonzero heritability" if it meets two criteria: (1) $h^2_{gene,t}$ 90%-CI > 0 and (2) 90%-CI > 0 for at least one MAF component ($h^2_{gene,r}$, $h^2_{gene,lf}$, or $h^2_{gene,c}$). Using this definition, the number of nonzero-h^2 genes ranges from 1,103 (7%) for corneal hysteresis to 2,258 (14%) for height (Table 1). Most of the estimated posterior means for these genes lie between 10^{-6} and 10^{-4} (Figure S20). While the number of genes passing the 90%-CI > 0 threshold is a biased estimator of polygenicity (Figure S14B), we can relatively reliably estimate the number of genes that explain 50% of the trait's cumulative gene-level heritability (Figure S15, material and methods). These estimates vary widely across traits, ranging from seven genes for hair color and sex hormone binding globulin concentration (SHBG) to 677 for BMI (Table 1).

We confirm that the approximation $\hat{h}^2_{gene,t} \approx \hat{h}^2_{gene,c} + \hat{h}^2_{gene,lf} + \hat{h}^2_{gene,r}$ is largely satisfied in real data; the average Pearson correlation across traits between $\hat{h}^2_{gene,t}$ and $\hat{h}^2_{gene,c} + \hat{h}^2_{gene,lf} + \hat{h}^2_{gene,r}$ is 0.97 (SD 0.05)

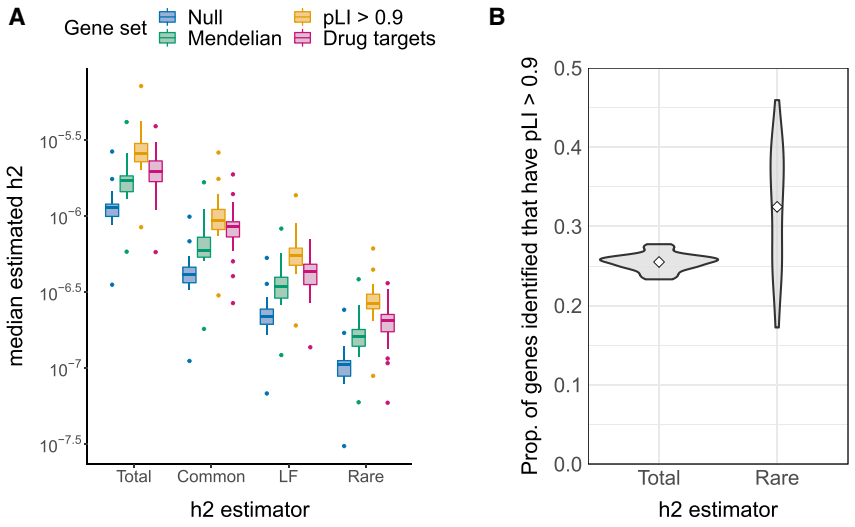

Figure 5. Genes of known biological importance have higher h^2 estimates

(A) Distributions of h^2 estimates for three gene sets: Mendelian-disorder genes (n = 2,971), LoF-intolerant genes (pLI > 0.9, n = 2,562), and immune-related drug targets (n = 176). Each point is the median posterior mean across genes for a given trait; each boxplot represents 25 traits.

(B) Proportion of nonzero-h^2 genes identified at 90%-CI > 0 for $h^2_{\text{gene},t}$ and $h^2_{\text{gene},r}$ that are putatively LoF intolerant. Each violin plot is a distribution across 25 traits. For reference, genes with pLI > 0.9 comprise 16% of all genes in the analysis.

(Figure S21). As expected, $\widehat{h}^2_{\text{gene,c}}$ behaves similarly to $\widehat{h}^2_{\text{gene,t}}$. The average Pearson R^2 of $\widehat{h}^2_{\text{gene,c}}$ and $\widehat{h}^2_{\text{gene,t}}$ across the 25 traits is 94% (SD 1%) (Figure S22). 92% (SD 1%) of nonzero-heritability genes have significant common-variant heritability; 76% (SD 1%) have significant causal effects exclusively from common variants (Table 1). On the other hand, $\widehat{h}^2_{\text{gene,r}}$ is significantly less correlated with $\widehat{h}^2_{\text{gene,t}}$ (average Pearson R^2 = 30% [SD 21%] across traits) (Figure S22). Approximately 2.5% (SD 0.6%) of genes have significant rare-variant heritability (Table S3), and only 0.8% (SD 0.4%)—327 gene-trait pairs in total—have significant heritability exclusively from rare variants (Table 1, Table S4).

LoF-intolerant genes are strongly enriched among genes with only rare-variant heritability

We estimate, and partition by MAF, the gene-level heritabilities of (1) known Mendelian-disorder genes from OMIM[69] (n = 2,971), (2) loss-of-function (LoF)-intolerant genes (probability of LoF-intolerance [pLI] > 0.9)[48] (n = 2,562), and (3) a set of FDA-approved drug targets for 30 immune-related traits[70] (n = 176) (material and methods). Compared to a set of "null" genes (sampled from the set of genes not contained in any of the three gene sets), all three gene sets have significantly higher median estimates of total and MAF-partitioned gene-level heritability (Figure 5A).

The Mendelian-disorder gene set comprises 19% of all genes and is enriched for genes with $h^2_{\text{gene,r}}$ 90%-CI > 0 for at least one trait (Fisher's exact test, OR and 95%-CI: 1.4 [1.1, 1.7], Table S3) but not for nonzero-$h^2_{\text{gene,t}}$ genes (OR = 1.1 [1.0, 1.2]) or genes with exclusively rare-variant heritability (OR = 1.1 [0.8, 1.5], Table S4). In contrast, the LoF-intolerant genes comprise 16% of all genes and are enriched for nonzero-$h^2_{\text{gene,t}}$ genes (OR and 95%-CI: 1.4 [1.3, 1.5]), nonzero-$h^2_{\text{gene,r}}$ genes (OR = 1.5 [1.2, 1.8], Table S3), and genes with exclusively rare-variant heritability (OR = 1.6 [1.2, 2.2], Table S4). On average across traits, 26% (SD 1%) of the genes identified at $h^2_{\text{gene,t}}$ 90%-CI > 0; 33% (SD 8%) of those with $h^2_{\text{gene,r}}$ 90%-CI > 0; and 35% (SD 20%) of those with exclusively rare-variant heritability are also LoF-intolerant (Figure 5B).

Of the 327 gene-trait pairs with only rare-variant heritability (ranging from three genes for heel T-score and corneal hysteresis to 27 genes for height [Table 1, Table S4]), 213 gene-trait pairs are also identified by MAGMA[71] (FDR < 0.05, material and methods). We observe a 1.6× enrichment of LoF-intolerant genes among the gene-trait pairs identified by both methods and a 2.3× enrichment among the gene-trait pairs identified by only our method, indicating that the genes identified by only our method are indeed capturing meaningful signal. The 114 additional gene-trait pairs found by our method (Table S5) include six unique genes (seven gene-trait pairs) with estimated posterior means $\widehat{h}^2_{\text{gene,r}} > 10^{-4}$. Of these six genes, three are LoF-intolerant: *DYNC1LI2*, identified for MSCV ($h^2_{\text{gene,r}}$ 90%-CI = [2e−4, 4e−4], MAGMA *Z* score = 2.1, pLI = 1, recently implicated in cystinosis, a lysosomal storage disorder[72]); *ARHGAP25*, identified for monocyte count ($h^2_{\text{gene,r}}$ 90%-CI = [9e−5, 3e−4], MAGMA *Z* score = 2.1, pLI = 0.95, has known roles in phagocytosis[73,74]); and *PHC3*, identified for basal metabolic rate ($h^2_{\text{gene,r}}$ 90%-CI = [7e−5, 2e−4], MAGMA *Z* score = 1.9, pLI = 1, implicated in osteosarcoma[75,76]).

$h^2_{\text{gene,r}}$ identifies genes that link complex traits to phenotypically related monogenic disorders

Among the 1,050 gene-trait pairs identified at $h^2_{\text{gene,r}}$ 90%-CI > 0 (Table S3), 161 have $h^2_{\text{gene,r}}$ 90%-CI > 10^{-4}. Several of these genes with large rare-variant heritability are implicated in Mendelian disorders that are phenotypically related to the complex trait. For example, the gene with the largest rare-variant heritability we identify is *MPDU1* for SHBG concentration, a liver-secreted glycoprotein[77] ($h^2_{\text{gene,r}}$ 90%-CI = [0.020, 0.021]); certain mutations in *MPDU1* are known to cause a congenital disorder of glycosylation,[78,79] and there is evidence that MPDU1 interacts

with SHBG.[80] *IL17RA*, identified for monocyte count ($h^2_{\text{gene,r}}$ 90%-CI = [0.0040, 0.0048]), is involved in an autosomal recessive immunodeficiency disorder.[81,82] *GFI1B*, identified for mean platelet volume ($h^2_{\text{gene,r}}$ 90%-CI = [0.0037, 0.0044]), is involved in platelet-type bleeding disorder-17, an autosomal dominant disorder characterized by increased bleeding due to abnormal platelet function.[83]

Although we did not find a statistically significant overlap between the Mendelian-disorder gene set and the set of genes with exclusively rare-variant heritability, the top genes (rank ordered by $\widehat{h}^2_{\text{gene,r}}$) among the 114 gene-trait pairs identified by our method and not by MAGMA (FDR < 0.05, Table S5) also include examples of genes that may link complex traits to phenotypically related monogenic disorders. For example, we identify *AKT2* for serum gamma-glutamyl transferase concentration (GGT) (90%-CI of $h^2_{\text{gene,r}}$ = [3e−5, 1e−4]), which is used to test for the presence of liver disease; *AKT2* is implicated in monogenic forms of type 2 diabetes[84] and hypoinsulinemic hypoglycemia with hemihypertrophy.[85] The *AKT2* annotation used for this analysis contains 24 rare variants, of which, 1 is identified as causal. For serum apolipoprotein A1, we identify *VPS13D* ($h^2_{\text{gene,r}}$ 90%-CI = [4e−5, 2e−4]; annotation contains 119 are rare variants, of which ∼2 are identified as causal). Compound heterozygous mutations in *VPS13D* are known to cause an autosomal recessive ataxia characterized in part by abnormal mitochondrial morphology, reduced energy generation, and lipidosis,[86,87] and VPS13D was recently shown to have direct involvement in trafficking fatty acids from lipid droplets to mitochondria.[88]

Our results are consistent with the hypothesis that complex-trait variation may be explained in part by dysregulation of genes that—if completely disrupted—cause phenotypically similar or related Mendelian disorders.[54] We emphasize that, because heritability reflects genetic and phenotypic variation at the population level, if a common variant and rare variant explain the same heritability (i.e., have the same standardized causal effect size), the *allelic* effect—the expected change in phenotype per additional copy of the effect allele—is significantly larger for the rare variant.

MAF-partitioned gene-level heritability reveals unique insights into genetic architecture

We investigated whether gene-level heritability estimates are correlated with gene length, average LD score of variants in the gene (a proxy for the strength of LD in the region), and average MAF of variants in the gene. $\widehat{h}^2_{\text{gene,c}}$ (and, to a large extent, $\widehat{h}^2_{\text{gene,lf}}$) is distributed very similarly to $\widehat{h}^2_{\text{gene,t}}$ with respect to these variables (Figure 6, Figure S23). However, the distribution of $\widehat{h}^2_{\text{gene,r}}$ shows marked differences, particularly with respect to gene length. Specifically, we observe a higher average $\widehat{h}^2_{\text{gene,r}}$ among shorter genes even though the number of causal variants per gene (across all allele frequencies) increases with gene length (Figure 6, Figure S24). The expected per-causal variant effect size per gene is invariant to gene length for common and low-frequency variants, but for rare variants, the average across gene-trait pairs is nearly 10^{-4} in the shortest quintile of genes versus 10^{-6} in the longest (Figure 6).

Using the empirical distributions of cumulative $h^2_{\text{gene,t}}$, $h^2_{\text{gene,c}}$, $h^2_{\text{gene,lf}}$, and $h^2_{\text{gene,r}}$, we loosely quantify differences in polygenicity at the level of genes (with the caveat that, because there is a high degree of gene overlap in some regions, cumulative $h^2_{\text{gene,t}}$ may be more informative for some traits over others). For example, if cumulative $h^2_{\text{gene,t}}$ is divided equally across all genes, the empirical cumulative distribution function (CDF) for $h^2_{\text{gene,t}}$ would be the line $y = x$, where the x axis is the rank ordering of genes from highest to lowest $\widehat{h}^2_{\text{gene,t}}$; two traits with the same empirical CDF for $h^2_{\text{gene,t}}$ can have different empirical CDFs for each MAF-partitioned component. Once again, we find that the empirical CDFs of $h^2_{\text{gene,c}}$ are extremely similar to those of $h^2_{\text{gene,t}}$ (Figure 7, Figure S25). Although the curves generally have similar shapes across traits (i.e., similar spread of heritability across genes), some traits have a notable amount of heritability concentrated in just the top gene, and many of these gene-trait pairs have been functionally validated in the literature. For example, for urate, *SLC2A9*—a known urate transporter[89–91]—is the single largest contributor to total, common-, and LF-variant gene-level heritability ($\widehat{h}^2_{\text{gene,t}}$ = 0.062, $\widehat{h}^2_{\text{gene,c}}$ = 0.060, $\widehat{h}^2_{\text{gene,lf}}$ = 0.0034, $\widehat{h}^2_{\text{gene,r}}$ = 0), accounting for 32%, 39%, and 12% of the cumulative heritability for each estimand, respectively (Figure 7). For alkaline phosphatase, we find that *ALPL*—which encodes the enzyme alkaline phosphatase—is the single largest contributor to total and LF-variant gene-level heritability ($\widehat{h}^2_{\text{gene,t}}$ = 0.041, $\widehat{h}^2_{\text{gene,c}}$ = 0.018, $\widehat{h}^2_{\text{gene,lf}}$ = 0.021, $\widehat{h}^2_{\text{gene,r}}$ = 0), explaining 13% and 29% of the respective cumulative heritability estimands (Figure 7).

Discussion

We propose a general approach for estimating the heritability explained by any set of variants much smaller than an LD block and assess its utility in estimating/partitioning gene-level heritability. In simulations, we confirm that incorporating uncertainty about which variants are causal and what their effect sizes are dramatically improves specificity over naive approaches that ignore uncertainty in the causal effects. For 25 complex traits and >15K genes, we estimate gene-level heritability—the heritability explained by variants in the gene body plus a 10-kb window upstream/downstream of the gene start/end positions—and partition

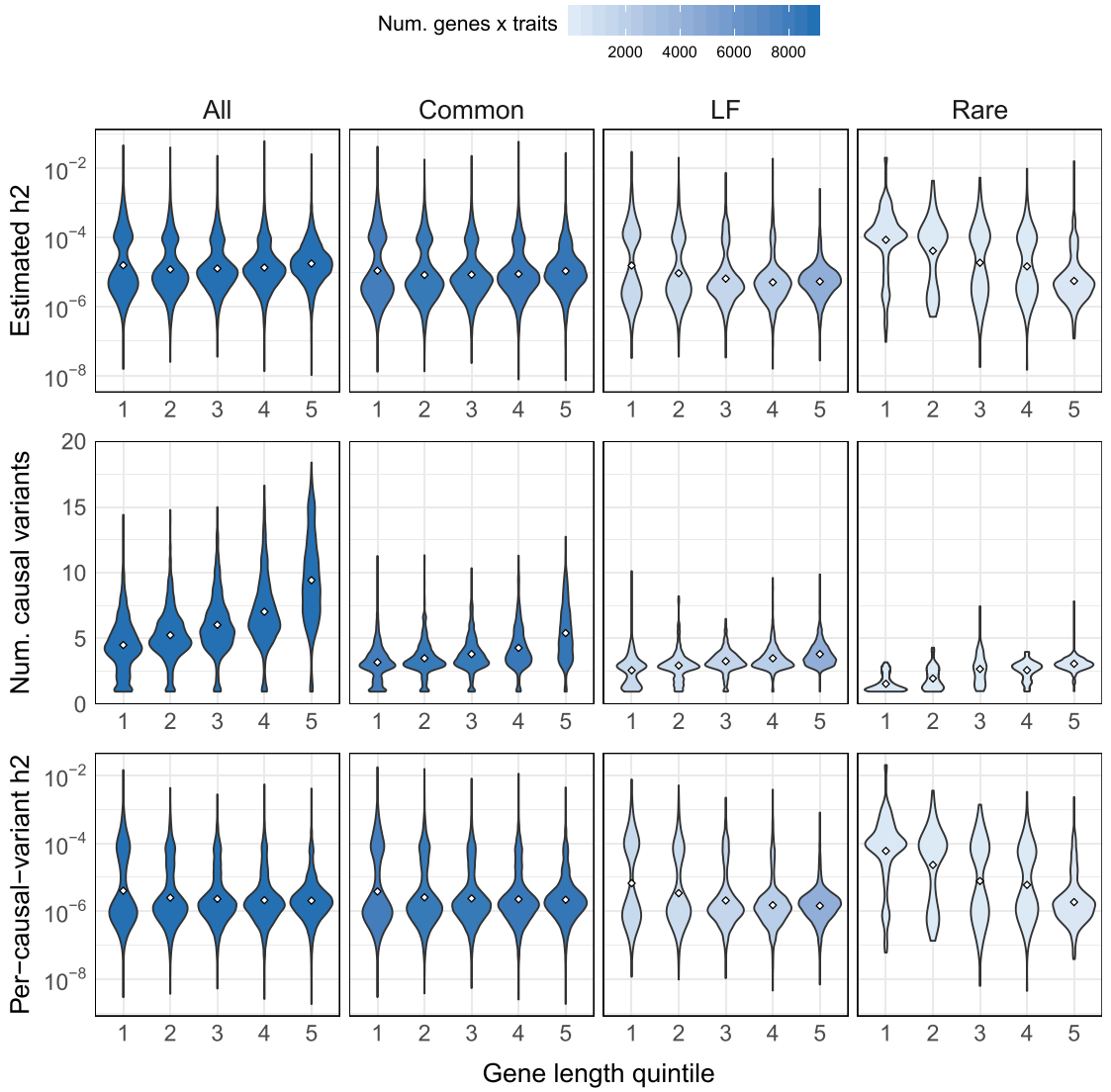

Figure 6. Inverse relationship between rare-variant h2 estimates and gene length
Estimates of h2 (top), number of causal variants per gene (middle), and expected effect size per causal variant per gene (bottom) with respect to gene length (x axis) for 25 traits. Each violin plot is the distribution of posterior mean estimates for nonzero-heritability genes with 90%-CIs > 0 for each h2 quantity. Color gradient indicates the number of estimates in each violin plot (number of gene-trait pairs).

by allele-frequency class to explore differences in genetic architecture across traits. As expected, most gene-level heritability is dominated by common variants, but we identify several genes per trait with nonzero heritability exclusively from rare or low-frequency variants. Notably, we find many genes with only rare-variant heritability that existing methods are underpowered to detect; these genes include LoF-intolerant genes and genes with known roles in Mendelian disorders that are phenotypically similar or related to the complex trait. Our results demonstrate that the rare-variant contribution to total gene-level heritability is a useful quantity that can be considered alongside common-variant heritability enrichments to obtain a more comprehensive understanding of genetic architecture.

We conclude by discussing the limitations of our approach. First, it is critical to remember that gene-level heritability is not an intrinsic property of a trait or gene. Like all "types" of heritability, estimates of total and MAF-partitioned gene-level heritability are only meaningful when considered in the populations in which they were measured.[45,46] Our real-data results are therefore specific to the population from which the "White British" individuals in the UK Biobank are sampled. In addition, genes with credible intervals > 0 must not be interpreted as "causal" without additional functional validation, as nonzero gene-level heritability indicates association—not causality.[51]

Second, multiple lines of evidence suggest that rare and "ultra-rare" variants, which are not well tagged by variants on genotyping arrays, may explain much of the "missing heritability" not captured by genotyped or imputed variants.[12,63,92] Because imputed genotypes are noisier for rarer

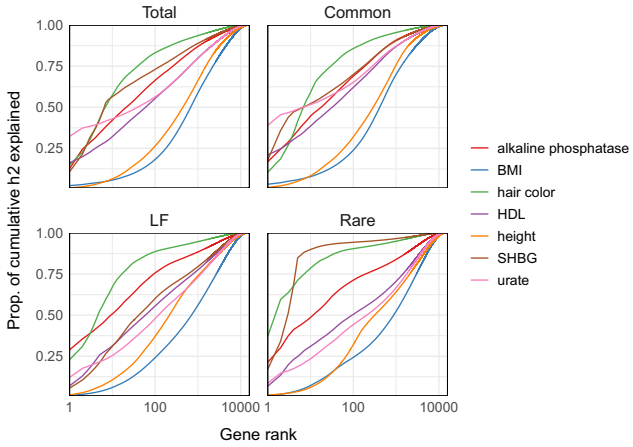

Figure 7. Gene-level heritability estimates capture differences in polygenicity across traits

Empirical distributions of cumulative heritability for seven example traits (clockwise from top left: total, common, rare, and low-frequency). Each curve can be read as, "the top X genes, rank ordered by estimated posterior mean, explain proportion Y of the cumulative gene-level heritability for a given trait" (Figure S25 shows all 25 traits).

variants and variants in lower LD regions, we analyze variants with MAF $> 0.5\%$. Additional work is needed to assess the error incurred by using genotyped/imputed data in lieu of whole-genome sequencing (WGS) as well as the signal that is missed by excluding variants with MAF $< 0.5\%$. While our estimator can be applied to whole-exome sequencing (WES) data, LD between coding and noncoding regions would significantly inflate gene-level heritability estimates; LD between exonic and intronic variants could also cloud interpretation, depending on the application. With multiple biobanks starting to sequence large numbers of individuals,[93–95] we believe the availability of large-scale WGS data will gradually become less of an issue.

We corrected for population structure by using genome-wide PCs (precomputed and provided by the UK Biobank in their data release[47]) as covariates in each GWAS. This is a standard approach to correcting for population stratification, which typically reflects geographic separation, in estimates of genome-wide SNP-heritability and genome-wide functional enrichments, both of which are driven by common SNPs. However, rare variants generally have more complex spatial distributions and thus exhibit stratification patterns distinct from those of common SNPs.[62,63] It is unclear whether methods that are effective for controlling stratification of common SNPs are applicable to rare variants.[96] While we did perform additional quality control to reduce potential false positives due to uncorrected rare-variant population structure, we leave a thorough investigation of the impact of recent and/or fine-scale structure for future work.

Our approach requires OLS association statistics and LD computed from a subset of individuals in the GWAS. While estimates of gene-level heritability and the MAF-partitioned components are robust to sample sizes as low as 5,000, the individuals used to estimate LD must be a subset of the individuals in the GWAS. Although summary association statistics are publicly available for hundreds of large-scale GWASs, most of these studies are meta-analyses and therefore do not have in-sample LD available. Moreover, many publicly available summary statistics were computed from linear mixed models rather than OLS, which is used throughout our simulations and derivations. Additional work is needed to extend our approach to allow external reference panel LD (e.g., 1000 Genomes[57]) and/or mixed model association statistics. Biobanks can help to ameliorate potential issues stemming from noisy LD by releasing summary LD information alongside summary association statistics.[97]

Finally, gene-level heritabilities of different genes can have nonzero covariance due to physical overlap between genes and/or correlated causal effect sizes.[98] In this work, we assume there is zero covariance between causal effects of different variants in order to facilitate inference. If, in fact, there is nonzero covariance between causal effects at different loci, total SNP-heritability would also include a nonzero covariance between the gene and its complement[43–46] (material and methods). Depending on whether the covariance is positive or negative, the gene-level heritability estimates from our method can be biased downward or upward. Thus, the heritability estimates for real traits reported in this work have additional sources of noise/uncertainty which were not directly modeled or accounted for. Since modeling correlation of causal effect sizes would make inference considerably more challenging, we leave this for future work.

Data and code availability

h2gene software and analysis scripts are available at https://github.com/bogdanlab/h2gene.

Supplemental information

Supplemental information can be found online at https://doi.org/10.1016/j.ajhg.2022.02.012.

Acknowledgments

We thank the UK Biobank Resource (application #33297) for making this work possible. We are also grateful to Alkes Price, Gregor Gorjanc, Harold Pimentel, Luke O'Connor, Nasa Sinnott-Armstrong, and Ruth Johnson for providing helpful comments and discussion. This work was funded in part by the National Institutes of Health under awards R01-HG009120 and R01-MH115676.

Declaration of interests

H.S. is now an employee of Genentech and holds stock in Roche.

Received: August 19, 2021
Accepted: February 15, 2022
Published: March 9, 2022

Web resources

LoF-intolerance metrics by gene, https://gnomad.broadinstitute.org/downloads
MAGMA software, https://ctg.cncr.nl/software/magma
OMIM gene list, https://github.com/bogdanlab/gene_sets/blob/master/mendelian_genes.bed
PLINK software, https://www.cog-genomics.org/plink2
Protein-coding gene list and coordinates, https://ctg.cncr.nl/software/magma
susieR software, https://github.com/stephenslab/susieR
UK Biobank Resource, https://www.ukbiobank.ac.uk/

References

1. Maurano, M.T., Humbert, R., Rynes, E., Thurman, R.E., Haugen, E., Wang, H., Reynolds, A.P., Sandstrom, R., Qu, H., Brody, J., et al. (2012). Systematic localization of common disease-associated variation in regulatory DNA. Science *337*, 1190–1195.
2. Pickrell, J.K. (2014). Joint analysis of functional genomic data and genome-wide association studies of 18 human traits. Am. J. Hum. Genet. *94*, 559–573.
3. Finucane, H.K., Bulik-Sullivan, B., Gusev, A., Trynka, G., Reshef, Y., Loh, P.-R., Anttila, V., Xu, H., Zang, C., Farh, K., et al. (2015). Partitioning heritability by functional annotation using genome-wide association summary statistics. Nat. Genet. *47*, 1228–1235.
4. Wray, N.R., Wijmenga, C., Sullivan, P.F., Yang, J., and Visscher, P.M. (2018). Common disease is more complex than implied by the core gene omnigenic model. Cell *173*, 1573–1580.
5. Boyle, E.A., Li, Y.I., and Pritchard, J.K. (2017). An expanded view of complex traits: From polygenic to omnigenic. Cell *169*, 1177–1186.
6. Liu, X., Li, Y.I., and Pritchard, J.K. (2019). Trans effects on gene expression can drive omnigenic inheritance. Cell *177*, 1022–1034.e6.
7. Bomba, L., Walter, K., and Soranzo, N. (2017). The impact of rare and low-frequency genetic variants in common disease. Genome Biol. *18*, 77.
8. Yao, C., Joehanes, R., Johnson, A.D., Huan, T., Liu, C., Freedman, J.E., Munson, P.J., Hill, D.E., Vidal, M., and Levy, D. (2017). Dynamic role of trans regulation of gene expression in relation to complex traits. Am. J. Hum. Genet. *100*, 985–986.
9. Caballero, A., Tenesa, A., and Keightley, P.D. (2015). The nature of genetic variation for complex traits revealed by GWAS and regional heritability mapping analyses. Genetics *201*, 1601–1613.
10. Golan, D., Lander, E.S., and Rosset, S. (2014). Measuring missing heritability: inferring the contribution of common variants. Proc. Natl. Acad. Sci. USA *111*, E5272–E5281.
11. Eyre-Walker, A. (2010). Genetic architecture of a complex trait and its implications for fitness and genome-wide association studies. Proc. Natl. Acad. Sci. USA *107* (*Suppl 1*), 1752–1756.
12. Wainschtein, P., Jain, D., Zheng, Z., Cupples, L.A., Shadyab, A.H., McKnight, B., et al. (2021). Recovery of trait heritability from whole genome sequence data. Prepint at bioRxiv. https://doi.org/10.1101/588020.
13. Yang, J., Benyamin, B., McEvoy, B.P., Gordon, S., Henders, A.K., Nyholt, D.R., Madden, P.A., Heath, A.C., Martin, N.G., Montgomery, G.W., et al. (2010). Common SNPs explain a large proportion of the heritability for human height. Nat. Genet. *42*, 565–569.
14. Hunt, K.A., Mistry, V., Bockett, N.A., Ahmad, T., Ban, M., Barker, J.N., Barrett, J.C., Blackburn, H., Brand, O., Burren, O., et al. (2013). Negligible impact of rare autoimmune-locus coding-region variants on missing heritability. Nature *498*, 232–235.
15. Yao, D.W., O'Connor, L.J., Price, A.L., and Gusev, A. (2020). Quantifying genetic effects on disease mediated by assayed gene expression levels. Nat. Genet. *52*, 626–633.
16. O'Connor, L.J., Schoech, A.P., Hormozdiari, F., Gazal, S., Patterson, N., and Price, A.L. (2019). Extreme polygenicity of complex traits is explained by negative selection. Am. J. Hum. Genet. *105*, 456–476.
17. Simons, Y.B., Bullaughey, K., Hudson, R.R., and Sella, G. (2018). A population genetic interpretation of GWAS findings for human quantitative traits. PLoS Biol. *16*, e2002985.
18. Gusev, A., Bhatia, G., Zaitlen, N., Vilhjalmsson, B.J., Diogo, D., Stahl, E.A., Gregersen, P.K., Worthington, J., Klareskog, L., Raychaudhuri, S., et al. (2013). Quantifying missing heritability at known GWAS loci. PLoS Genet. *9*, e1003993.
19. Marouli, E., Graff, M., Medina-Gomez, C., Lo, K.S., Wood, A.R., Kjaer, T.R., Fine, R.S., Lu, Y., Schurmann, C., Highland, H.M., et al. (2017). Rare and low-frequency coding variants alter human adult height. Nature *542*, 186–190.
20. Gusev, A., Ko, A., Shi, H., Bhatia, G., Chung, W., Penninx, B.W.J.H., Jansen, R., de Geus, E.J.C., Boomsma, D.I., Wright, F.A., et al. (2016). Integrative approaches for large-scale transcriptome-wide association studies. Nat. Genet. *48*, 245–252.
21. Wainberg, M., Sinnott-Armstrong, N., Mancuso, N., Barbeira, A.N., Knowles, D.A., Golan, D., Ermel, R., Ruusalepp, A., Quertermous, T., Hao, K., et al. (2019). Opportunities and challenges for transcriptome-wide association studies. Nat. Genet. *51*, 592–599.
22. Ionita-Laza, I., Lee, S., Makarov, V., Buxbaum, J.D., and Lin, X. (2013). Sequence kernel association tests for the combined effect of rare and common variants. Am. J. Hum. Genet. *92*, 841–853.
23. Wu, M.C., Lee, S., Cai, T., Li, Y., Boehnke, M., and Lin, X. (2011). Rare-variant association testing for sequencing data with the sequence kernel association test. Am. J. Hum. Genet. *89*, 82–93.
24. Price, A.L., Kryukov, G.V., de Bakker, P.I.W., Purcell, S.M., Staples, J., Wei, L.-J., and Sunyaev, S.R. (2010). Pooled association tests for rare variants in exon-resequencing studies. Am. J. Hum. Genet. *86*, 832–838.
25. Zuk, O., Schaffner, S.F., Samocha, K., Do, R., Hechter, E., Kathiresan, S., Daly, M.J., Neale, B.M., Sunyaev, S.R., and Lander, E.S. (2014). Searching for missing heritability: designing rare variant association studies. Proc. Natl. Acad. Sci. USA *111*, E455–E464.
26. Moutsianas, L., Agarwala, V., Fuchsberger, C., Flannick, J., Rivas, M.A., Gaulton, K.J., Albers, P.K., McVean, G., Boehnke, M., Altshuler, D., McCarthy, M.I.; and GoT2D Consortium (2015). The power of gene-based rare variant methods to detect disease-associated variation and test hypotheses about complex disease. PLoS Genet. *11*, e1005165.
27. Liu, D.J., Peloso, G.M., Zhan, X., Holmen, O.L., Zawistowski, M., Feng, S., Nikpay, M., Auer, P.L., Goel, A., Zhang, H., et al.

(2014). Meta-analysis of gene-level tests for rare variant association. Nat. Genet. *46*, 200–204.
28. Lee, S., Abecasis, G.R., Boehnke, M., and Lin, X. (2014). Rare-variant association analysis: study designs and statistical tests. Am. J. Hum. Genet. *95*, 5–23.
29. Lee, S., Emond, M.J., Bamshad, M.J., Barnes, K.C., Rieder, M.J., Nickerson, D.A., Christiani, D.C., Wurfel, M.M., Lin, X.; and NHLBI GO Exome Sequencing Project—ESP Lung Project Team (2012). Optimal unified approach for rare-variant association testing with application to small-sample case-control whole-exome sequencing studies. Am. J. Hum. Genet. *91*, 224–237.
30. Lee, S., Wu, M.C., and Lin, X. (2012). Optimal tests for rare variant effects in sequencing association studies. Biostatistics *13*, 762–775.
31. Udler, M.S., Tyrer, J., and Easton, D.F. (2010). Evaluating the power to discriminate between highly correlated SNPs in genetic association studies. Genet. Epidemiol. *34*, 463–468.
32. Tibshirani, R. (1996). Regression shrinkage and selection via the lasso. J. R. Stat. Soc. *58*, 267–288.
33. Gamazon, E.R., Cox, N.J., and Davis, L.K. (2014). Structural architecture of SNP effects on complex traits. Am. J. Hum. Genet. *95*, 477–489.
34. Shi, H., Kichaev, G., and Pasaniuc, B. (2016). Contrasting the genetic architecture of 30 complex traits from summary association data. Am. J. Hum. Genet. *99*, 139–153.
35. Benner, C., Havulinna, A.S., Salomaa, V., Ripatti, S., and Pirinen, M. (2018). Refining fine-mapping: effect sizes and regional heritability. Preprint at bioRxiv. https://doi.org/10.1101/318618.
36. Gusev, A., Lee, S.H., Trynka, G., Finucane, H., Vilhjálmsson, B.J., Xu, H., Zang, C., Ripke, S., Bulik-Sullivan, B., Stahl, E., et al. (2014). Partitioning heritability of regulatory and cell-type-specific variants across 11 common diseases. Am. J. Hum. Genet. *95*, 535–552.
37. Loh, P.-R., Bhatia, G., Gusev, A., Finucane, H.K., Bulik-Sullivan, B.K., Pollack, S.J., de Candia, T.R., Lee, S.H., Wray, N.R., Kendler, K.S., et al. (2015). Contrasting genetic architectures of schizophrenia and other complex diseases using fast variance-components analysis. Nat. Genet. *47*, 1385–1392.
38. Gazal, S., Loh, P.-R., Finucane, H.K., Ganna, A., Schoech, A., Sunyaev, S., and Price, A.L. (2018). Functional architecture of low-frequency variants highlights strength of negative selection across coding and non-coding annotations. Nat. Genet. *50*, 1600–1607.
39. Pazokitoroudi, A., Wu, Y., Burch, K.S., Hou, K., Zhou, A., Pasaniuc, B., and Sankararaman, S. (2020). Efficient variance components analysis across millions of genomes. Nat. Commun. *11*, 4020.
40. Speed, D., and Balding, D.J. (2019). SumHer better estimates the SNP heritability of complex traits from summary statistics. Nat. Genet. *51*, 277–284.
41. Yang, J., Bakshi, A., Zhu, Z., Hemani, G., Vinkhuyzen, A.A.E., Lee, S.H., Robinson, M.R., Perry, J.R.B., Nolte, I.M., van Vliet-Ostaptchouk, J.V., et al. (2015). Genetic variance estimation with imputed variants finds negligible missing heritability for human height and body mass index. Nat. Genet. *47*, 1114–1120.
42. Wang, G., Sarkar, A., Carbonetto, P., and Stephens, M. (2020). A simple new approach to variable selection in regression, with application to genetic fine mapping. J. R. Stat. Soc. Series B Stat. Methodol. *82*, 1273–1300.
43. de Los Campos, G., Sorensen, D., and Gianola, D. (2015). Genomic heritability: what is it? PLoS Genet. *11*, e1005048.
44. Gianola, D., de los Campos, G., Hill, W.G., Manfredi, E., and Fernando, R. (2009). Additive genetic variability and the Bayesian alphabet. Genetics *183*, 347–363.
45. Lehermeier, C., de Los Campos, G., Wimmer, V., and Schön, C.-C. (2017). Genomic variance estimates: With or without disequilibrium covariances? J. Anim. Breed. Genet. *134*, 232–241.
46. Schreck, N., Piepho, H.-P., and Schlather, M. (2019). Best prediction of the additive genomic variance in random-effects models. Genetics *213*, 379–394.
47. Bycroft, C., Freeman, C., Petkova, D., Band, G., Elliott, L.T., Sharp, K., Motyer, A., Vukcevic, D., Delaneau, O., O'Connell, J., et al. (2018). The UK Biobank resource with deep phenotyping and genomic data. Nature *562*, 203–209.
48. Lek, M., Karczewski, K.J., Minikel, E.V., Samocha, K.E., Banks, E., Fennell, T., O'Donnell-Luria, A.H., Ware, J.S., Hill, A.J., Cummings, B.B., et al. (2016). Analysis of protein-coding genetic variation in 60,706 humans. Nature *536*, 285–291.
49. Karczewski, K.J., Francioli, L.C., Tiao, G., Cummings, B.B., Alföldi, J., Wang, Q., Collins, R.L., Laricchia, K.M., Ganna, A., Birnbaum, D.P., et al. (2020). The mutational constraint spectrum quantified from variation in 141,456 humans. Nature *581*, 434–443.
50. Feldman, M.W., and Lewontin, R.C. (1975). The heritability hang-up. Science *190*, 1163–1168.
51. Lewontin, R.C. (1974). Annotation: the analysis of variance and the analysis of causes. Am. J. Hum. Genet. *26*, 400–411.
52. Shi, H., Burch, K.S., Johnson, R., Freund, M.K., Kichaev, G., Mancuso, N., Manuel, A.M., Dong, N., and Pasaniuc, B. (2020). Localizing components of shared transethnic genetic architecture of complex traits from GWAS summary data. Am. J. Hum. Genet. *106*, 805–817.
53. Shi, H., Gazal, S., Kanai, M., Koch, E.M., Schoech, A.P., Siewert, K.M., Kim, S.S., Luo, Y., Amariuta, T., Huang, H., et al. (2021). Population-specific causal disease effect sizes in functionally important regions impacted by selection. Nat. Commun. *12*, 1098.
54. Freund, M.K., Burch, K.S., Shi, H., Mancuso, N., Kichaev, G., Garske, K.M., Pan, D.Z., Miao, Z., Mohlke, K.L., Laakso, M., et al. (2018). Phenotype-specific enrichment of Mendelian disorder genes near GWAS regions across 62 complex traits. Am. J. Hum. Genet. *103*, 535–552.
55. Sorensen, D., Fernando, R., and Gianola, D. (2001). Inferring the trajectory of genetic variance in the course of artificial selection. Genet. Res. *77*, 83–94.
56. Lara, L.A.C., Pocrnic, I., Oliveira, T.P., Gaynor, R.C., and Gorjanc, G. (2022). Temporal and genomic analysis of additive genetic variance in breeding programmes. Heredity *128*, 21–32.
57. Auton, A., Brooks, L.D., Durbin, R.M., Garrison, E.P., Kang, H.M., Korbel, J.O., Marchini, J.L., McCarthy, S., McVean, G.A., Abecasis, G.R.; and 1000 Genomes Project Consortium (2015). A global reference for human genetic variation. Nature *526*, 68–74.
58. Berisa, T., and Pickrell, J.K. (2016). Approximately independent linkage disequilibrium blocks in human populations. Bioinformatics *32*, 283–285.
59. Speed, D., Cai, N., Johnson, M.R., Nejentsev, S., Balding, D.J.; and UCLEB Consortium (2017). Reevaluation of SNP heritability in complex human traits. Nat. Genet. *49*, 986–992.

60. Hou, K., Burch, K.S., Majumdar, A., Shi, H., Mancuso, N., Wu, Y., Sankararaman, S., and Pasaniuc, B. (2019). Accurate estimation of SNP-heritability from biobank-scale data irrespective of genetic architecture. Nat. Genet. *51*, 1244–1251.
61. Galinsky, K.J., Bhatia, G., Loh, P.-R., Georgiev, S., Mukherjee, S., Patterson, N.J., and Price, A.L. (2016). Fast principal-component analysis reveals convergent evolution of ADH1B in Europe and east Asia. Am. J. Hum. Genet. *98*, 456–472.
62. Mathieson, I., and McVean, G. (2012). Differential confounding of rare and common variants in spatially structured populations. Nat. Genet. *44*, 243–246.
63. Young, A.I. (2019). Solving the missing heritability problem. PLoS Genet. *15*, e1008222.
64. Zaidi, A.A., and Mathieson, I. (2020). Demographic history mediates the effect of stratification on polygenic scores. eLife *9*, e61548.
65. Sinnott-Armstrong, N., Tanigawa, Y., Amar, D., Mars, N., Benner, C., Aguirre, M., Venkataraman, G.R., Wainberg, M., Ollila, H.M., Kiiskinen, T., et al. (2021). Genetics of 35 blood and urine biomarkers in the UK Biobank. Nat. Genet. *53*, 185–194.
66. Lusis, A.J., Fogelman, A.M., and Fonarow, G.C. (2004). Genetic basis of atherosclerosis: part I: new genes and pathways. Circulation *110*, 1868–1873.
67. Musunuru, K., Strong, A., Frank-Kamenetsky, M., Lee, N.E., Ahfeldt, T., Sachs, K.V., Li, X., Li, H., Kuperwasser, N., Ruda, V.M., et al. (2010). From noncoding variant to phenotype via SORT1 at the 1p13 cholesterol locus. Nature *466*, 714–719.
68. Sharma, U., Pal, D., and Prasad, R. (2014). Alkaline phosphatase: an overview. Indian J. Clin. Biochem. *29*, 269–278.
69. Amberger, J.S., Bocchini, C.A., Schiettecatte, F., Scott, A.F., and Hamosh, A. (2015). OMIM.org: Online Mendelian Inheritance in Man (OMIM®), an online catalog of human genes and genetic disorders. Nucleic Acids Res. *43*, D789–D798.
70. Fang, H., De Wolf, H., Knezevic, B., Burnham, K.L., Osgood, J., Sanniti, A., Lledó Lara, A., Kasela, S., De Cesco, S., Wegner, J.K., et al. (2019). A genetics-led approach defines the drug target landscape of 30 immune-related traits. Nat. Genet. *51*, 1082–1091.
71. de Leeuw, C.A., Mooij, J.M., Heskes, T., and Posthuma, D. (2015). MAGMA: generalized gene-set analysis of GWAS data. PLoS Comput. Biol. *11*, e1004219.
72. Rahman, F., Johnson, J.L., Zhang, J., He, J., Pestonjamasp, K., Cherqui, S., and Catz, S.D. (2021). DYNC1LI2 regulates localization of the chaperone-mediated autophagy receptor LAMP2A and improves cellular homeostasis in cystinosis. Autophagy. Published online October 13, 2021. https://doi.org/10.1080/15548627.2021.1971937.
73. Schlam, D., Bagshaw, R.D., Freeman, S.A., Collins, R.F., Pawson, T., Fairn, G.D., and Grinstein, S. (2015). Phosphoinositide 3-kinase enables phagocytosis of large particles by terminating actin assembly through Rac/Cdc42 GTPase-activating proteins. Nat. Commun. *6*, 8623.
74. Csépányi-Kömi, R., Sirokmány, G., Geiszt, M., and Ligeti, E. (2012). ARHGAP25, a novel Rac GTPase-activating protein, regulates phagocytosis in human neutrophilic granulocytes. Blood *119*, 573–582.
75. Iwata, S., Takenobu, H., Kageyama, H., Koseki, H., Ishii, T., Nakazawa, A., Tatezaki, S., Nakagawara, A., and Kamijo, T. (2010). Polycomb group molecule PHC3 regulates polycomb complex composition and prognosis of osteosarcoma. Cancer Sci. *101*, 1646–1652.
76. Sauvageau, M., and Sauvageau, G. (2010). Polycomb group proteins: multi-faceted regulators of somatic stem cells and cancer. Cell Stem Cell *7*, 299–313.
77. Thaler, M.A., Seifert-Klauss, V., and Luppa, P.B. (2015). The biomarker sex hormone-binding globulin - from established applications to emerging trends in clinical medicine. Best Pract. Res. Clin. Endocrinol. Metab. *29*, 749–760.
78. Kranz, C., Denecke, J., Lehrman, M.A., Ray, S., Kienz, P., Kreissel, G., Sagi, D., Peter-Katalinic, J., Freeze, H.H., Schmid, T., et al. (2001). A mutation in the human MPDU1 gene causes congenital disorder of glycosylation type If (CDG-If). J. Clin. Invest. *108*, 1613–1619.
79. Schenk, B., Imbach, T., Frank, C.G., Grubenmann, C.E., Raymond, G.V., Hurvitz, H., Korn-Lubetzki, I., Revel-Vik, S., Raas-Rotschild, A., Luder, A.S., et al. (2001). MPDU1 mutations underlie a novel human congenital disorder of glycosylation, designated type If. J. Clin. Invest. *108*, 1687–1695.
80. Pope, S.N., and Lee, I.R. (2005). Yeast two-hybrid identification of prostatic proteins interacting with human sex hormone-binding globulin. J. Steroid Biochem. Mol. Biol. *94*, 203–208.
81. Lévy, R., Okada, S., Béziat, V., Moriya, K., Liu, C., Chai, L.Y.A., Migaud, M., Hauck, F., Al Ali, A., Cyrus, C., et al. (2016). Genetic, immunological, and clinical features of patients with bacterial and fungal infections due to inherited IL-17RA deficiency. Proc. Natl. Acad. Sci. USA *113*, E8277–E8285.
82. Puel, A., Cypowyj, S., Bustamante, J., Wright, J.F., Liu, L., Lim, H.K., Migaud, M., Israel, L., Chrabieh, M., Audry, M., et al. (2011). Chronic mucocutaneous candidiasis in humans with inborn errors of interleukin-17 immunity. Science *332*, 65–68.
83. Monteferrario, D., Bolar, N.A., Marneth, A.E., Hebeda, K.M., Bergevoet, S.M., Veenstra, H., Laros-van Gorkom, B.A.P., MacKenzie, M.A., Khandanpour, C., Botezatu, L., et al. (2014). A dominant-negative GFI1B mutation in the gray platelet syndrome. N. Engl. J. Med. *370*, 245–253.
84. George, S., Rochford, J.J., Wolfrum, C., Gray, S.L., Schinner, S., Wilson, J.C., Soos, M.A., Murgatroyd, P.R., Williams, R.M., Acerini, C.L., et al. (2004). A family with severe insulin resistance and diabetes due to a mutation in AKT2. Science *304*, 1325–1328.
85. Hussain, K., Challis, B., Rocha, N., Payne, F., Minic, M., Thompson, A., Daly, A., Scott, C., Harris, J., Smillie, B.J.L., et al. (2011). An activating mutation of AKT2 and human hypoglycemia. Science *334*, 474.
86. Seong, E., Insolera, R., Dulovic, M., Kamsteeg, E.-J., Trinh, J., Brüggemann, N., Sandford, E., Li, S., Ozel, A.B., Li, J.Z., et al. (2018). Mutations in VPS13D lead to a new recessive ataxia with spasticity and mitochondrial defects. Ann. Neurol. *83*, 1075–1088.
87. Gauthier, J., Meijer, I.A., Lessel, D., Mencacci, N.E., Krainc, D., Hempel, M., Tsiakas, K., Prokisch, H., Rossignol, E., Helm, M.H., et al. (2018). Recessive mutations in VPS13D cause childhood onset movement disorders. Ann. Neurol. *83*, 1089–1095.
88. Wang, J., Fang, N., Xiong, J., Du, Y., Cao, Y., and Ji, W.-K. (2021). An ESCRT-dependent step in fatty acid transfer from lipid droplets to mitochondria through VPS13D-TSG101 interactions. Nat. Commun. *12*, 1252.
89. Vitart, V., Rudan, I., Hayward, C., Gray, N.K., Floyd, J., Palmer, C.N.A., Knott, S.A., Kolcic, I., Polasek, O., Graessler, J., et al. (2008). SLC2A9 is a newly identified urate transporter

influencing serum urate concentration, urate excretion and gout. Nat. Genet. *40*, 437–442.

90. Anzai, N., Ichida, K., Jutabha, P., Kimura, T., Babu, E., Jin, C.J., Srivastava, S., Kitamura, K., Hisatome, I., Endou, H., and Sakurai, H. (2008). Plasma urate level is directly regulated by a voltage-driven urate efflux transporter URATv1 (SLC2A9) in humans. J. Biol. Chem. *283*, 26834–26838.
91. Caulfield, M.J., Munroe, P.B., O'Neill, D., Witkowska, K., Charchar, F.J., Doblado, M., Evans, S., Eyheramendy, S., Onipinla, A., Howard, P., et al. (2008). SLC2A9 is a high-capacity urate transporter in humans. PLoS Med. *5*, e197.
92. Mancuso, N., Rohland, N., Rand, K.A., Tandon, A., Allen, A., Quinque, D., Mallick, S., Li, H., Stram, A., Sheng, X., et al. (2016). The contribution of rare variation to prostate cancer heritability. Nat. Genet. *48*, 30–35.
93. Younes, N., Syed, N., Yadav, S.K., Haris, M., Abdallah, A.M., and Abu-Madi, M. (2021). A whole-genome sequencing association study of low bone mineral density identifies new susceptibility loci in the phase I Qatar Biobank cohort. J. Pers. Med. *11*, 34.
94. Taliun, D., Harris, D.N., Kessler, M.D., Carlson, J., Szpiech, Z.A., Torres, R., Taliun, S.A.G., Corvelo, A., Gogarten, S.M., Kang, H.M., et al. (2021). Sequencing of 53,831 diverse genomes from the NHLBI TOPMed Program. Nature *590*, 290–299.
95. Turro, E., Astle, W.J., Megy, K., Gräf, S., Greene, D., Shamardina, O., Allen, H.L., Sanchis-Juan, A., Frontini, M., Thys, C., et al. (2020). Whole-genome sequencing of patients with rare diseases in a national health system. Nature *583*, 96–102.
96. Bhatia, G., Gusev, A., Loh, P.-R., Finucane, H., Vilhjálmsson, B.J., Ripke, S., Purcell, S., Stahl, E., Daly, M., de Candia, T.R., et al. (2016). Subtle stratification confounds estimates of heritability from rare variants. Preprint at bioRxiv. https://doi.org/10.1101/048181.
97. Weissbrod, O., Hormozdiari, F., Benner, C., Cui, R., Ulirsch, J., Gazal, S., Schoech, A.P., van de Geijn, B., Reshef, Y., Márquez-Luna, C., et al. (2020). Functionally informed fine-mapping and polygenic localization of complex trait heritability. Nat. Genet. *52*, 1355–1363.
98. Schoech, A.P., Weissbrod, O., O'Connor, L.J., Patterson, N., Shi, H., Reshef, Y., and Price, A.L. (2020). Negative short-range genomic autocorrelation of causal effects on human complex traits. Preprint at bioRxiv. https://doi.org/10.1101/2020.09.23.310748.

The American Journal of Human Genetics, Volume *109*

Supplemental information

Partitioning gene-level contributions to complex-trait heritability by allele frequency identifies disease-relevant genes

Kathryn S. Burch, Kangcheng Hou, Yi Ding, Yifei Wang, Steven Gazal, Huwenbo Shi, and Bogdan Pasaniuc

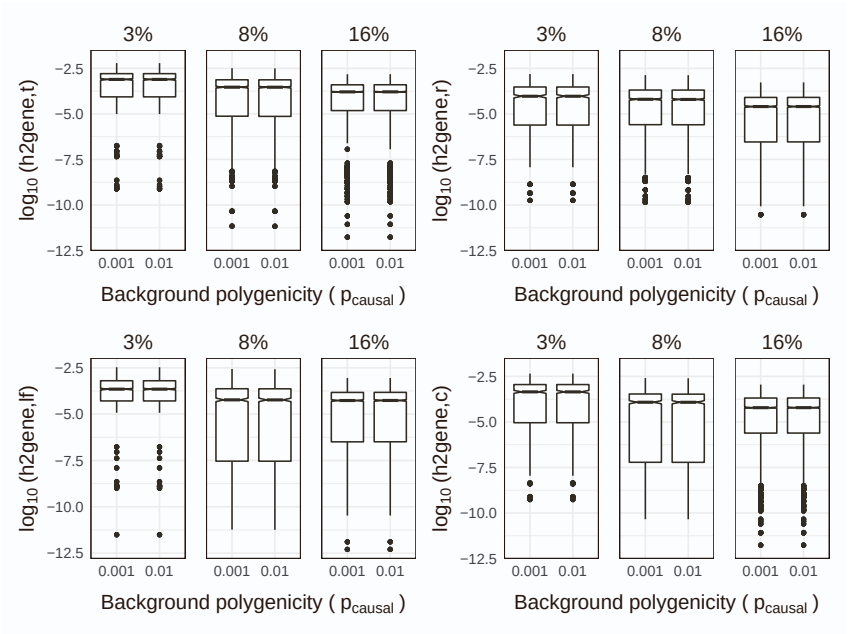

Supplementary Figure 1: Distributions of simulated values of $h^2_{\text{gene,t}}$, $h^2_{\text{gene,r}}$, $h^2_{\text{gene,lf}}$, and $h^2_{\text{gene,c}}$ in simulations on chromosome 1. Total $h^2_G = 0.05$. Cumulative $h^2_{\text{gene,t}} = 0.03$. 30 simulation replicates, MAF $>$ 0.005, N=291K. The proportion of causal genes (out of 1,083 genes on chr1) was set to 3%, 8%, or 16%. Background polygenicity was set to $p_{\text{causal}} = \{0.001, 0.01\}$.

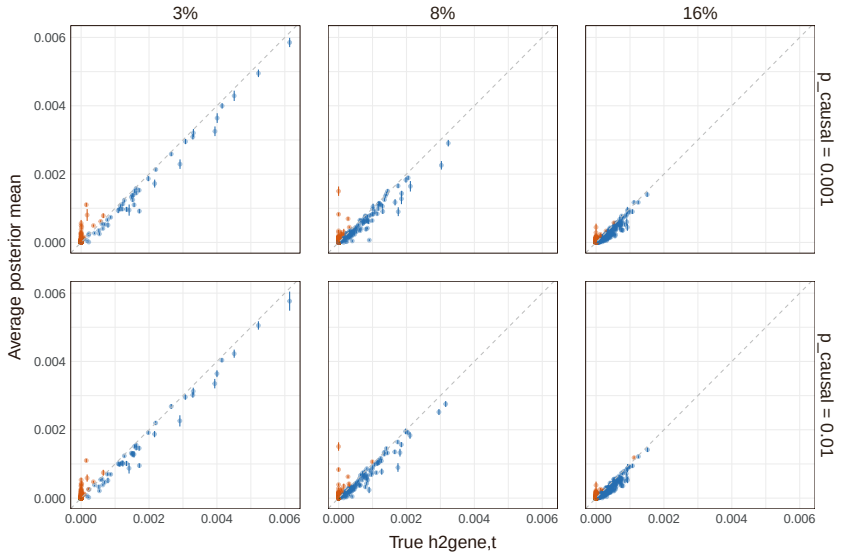

Supplementary Figure 2: Average $\hat{h}^2_{\text{gene,t}}$ vs. true $h^2_{\text{gene,t}}$ in simulations on chromosome 1 where 3% (left), 8% (middle), or 16% (right) of genes are causal. Orange points are genes with significantly upward-biased $\hat{h}^2_{\text{gene,t}}$, where bias is estimated as the average error, $(\hat{h}^2_{\text{gene}} - h^2_{\text{gene}})$, from 30 simulation replicates, and is considered "significant" if the error bars (± 1.96 s.e.m.) do not overlap true value of $h^2_{\text{gene,t}}$. Total $h^2_G = 0.05$. Cumulative $h^2_{\text{gene,t}} = 0.03$. MAF $>$ 0.005, N=291K.

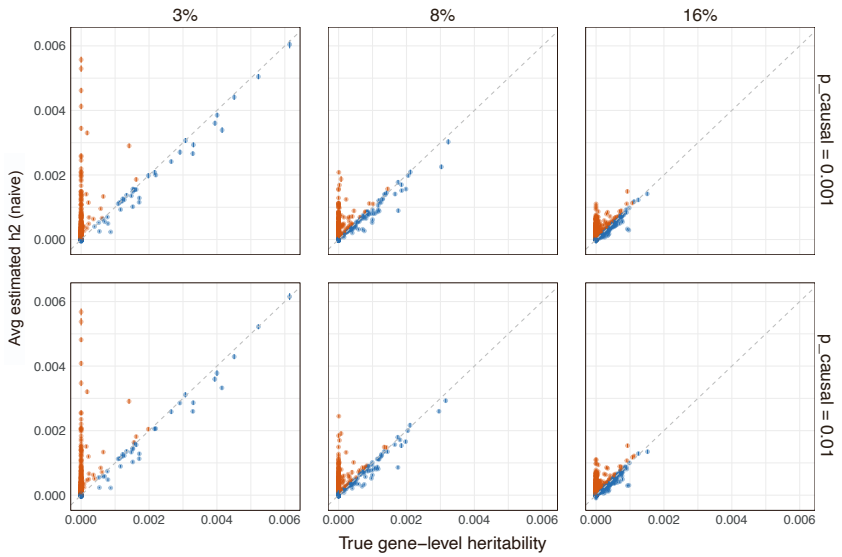

Supplementary Figure 3: Average estimated $h^2_{\text{gene,t}}$ from "naive method" vs. true value of $h^2_{\text{gene,t}}$ in simulations on chromosome 1 where 3%, 8%, or 16% of genes are causal. Orange points are genes with significantly upward-biased $\hat{h}^2_{\text{gene,t}}$, where bias is estimated as the average error, $(\hat{h}^2_{\text{gene}} - h^2_{\text{gene}})$, from 30 simulation replicates, and is considered "significant" if the error bars (± 1.96 s.e.m.) do not overlap true value of $h^2_{\text{gene,t}}$. Total $h^2_G = 0.05$, cumulative $h^2_{\text{gene,t}} = 0.03$, MAF $>$ 0.005, N=291K.

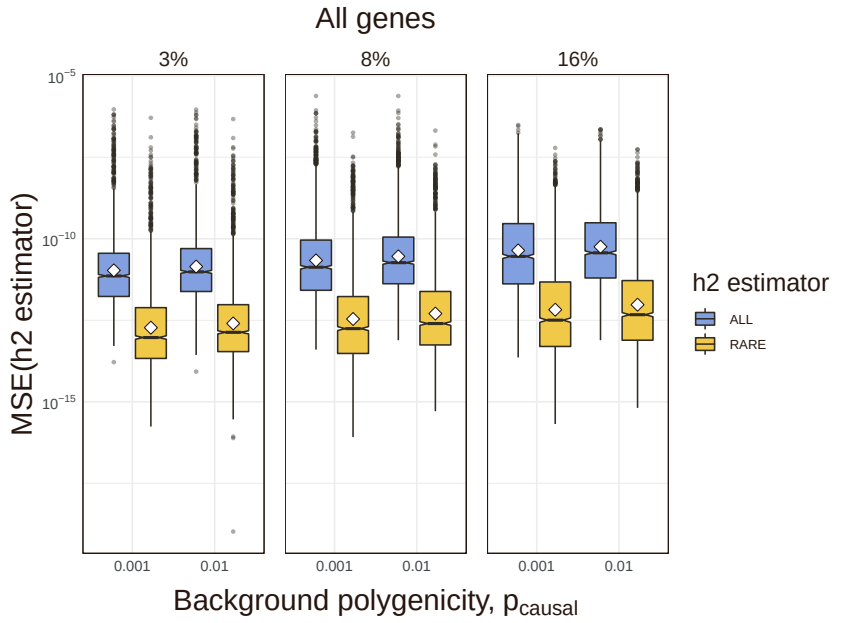

Supplementary Figure 4: MSE of $\hat{h}^2_{\text{gene,t}}$ (blue) and $\hat{h}^2_{\text{gene,r}}$ (yellow) for all 1,083 genes with respect to p_{causal} (x-axis) in simulations on chromosome 1 where either 3%, 8%, or 16% of genes are causal. Each point in each boxplot is the MSE for a single gene estimated from 30 simulation replicates. Total $h^2_G = 0.05$. Cumulative $h^2_{\text{gene,t}} = 0.03$, MAF $>$ 0.005, $N = 291K$.

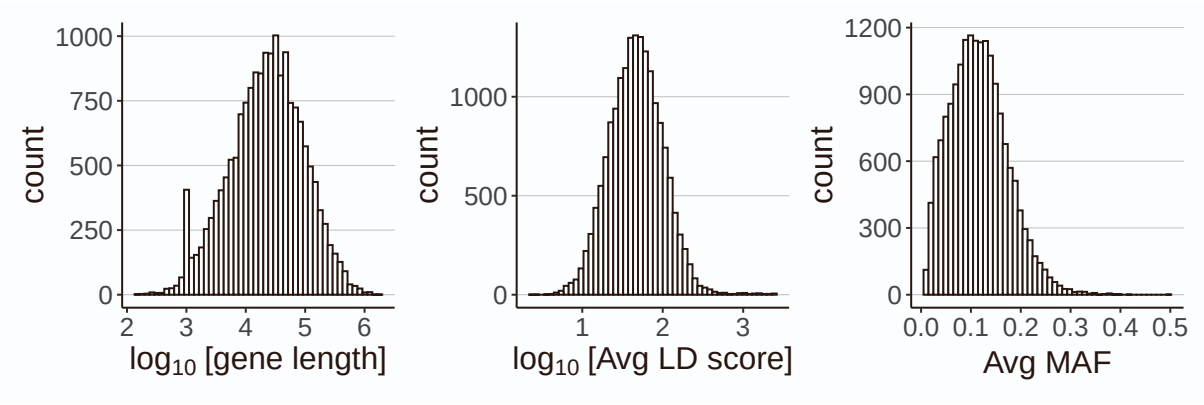

Supplementary Figure 5: Distribution of gene lengths (left), average LD score of variants assigned to gene (middle), and average MAF of variants assigned to gene (right) for 17,437 genes.

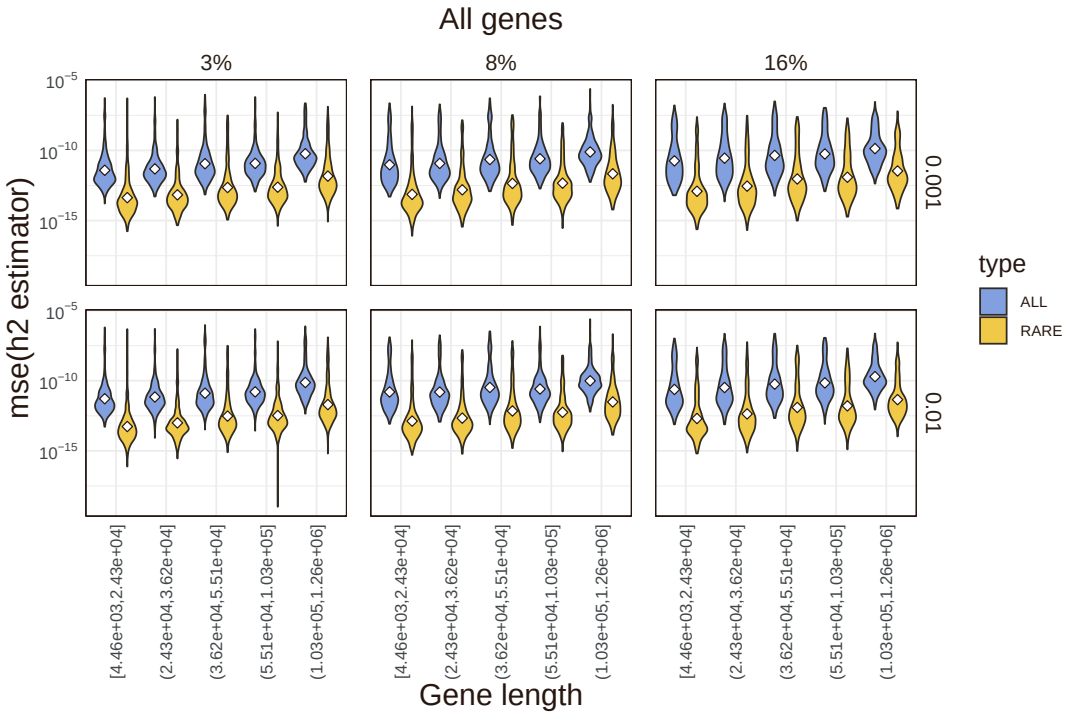

Supplementary Figure 6: MSE of $\hat{h}^2_{\text{gene,t}}$ (blue) and $\hat{h}^2_{\text{gene,r}}$ (yellow) with respect to gene length in simulations on chr1. Total $h^2_G = 0.05$. Cumulative $h^2_{\text{gene,t}} = 0.03$, MAF > 0.005, $N = 291K$, 30 simulation replicates.

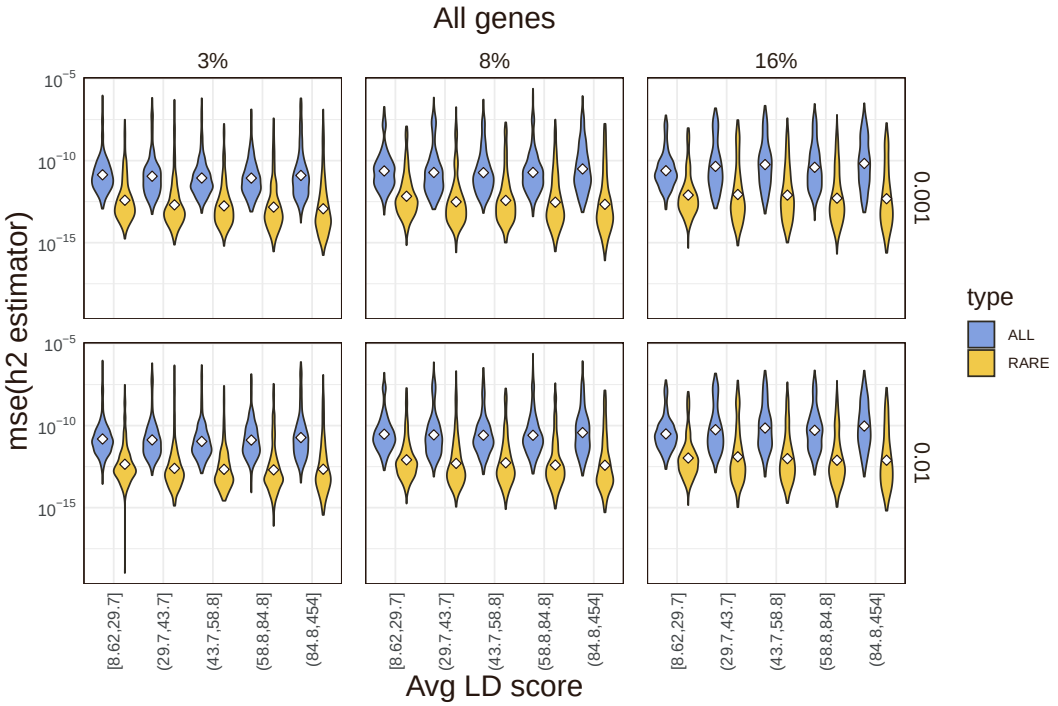

Supplementary Figure 7: MSE of $\hat{h}^2_{\text{gene,t}}$ (blue) and $\hat{h}^2_{\text{gene,r}}$ (yellow) with respect to average LD score of variants assigned to gene in simulations on chr1. Total $h^2_G = 0.05$. Cumulative $h^2_{\text{gene,t}} = 0.03$, MAF $>$ 0.005, $N = 291K$, 30 simulation replicates.

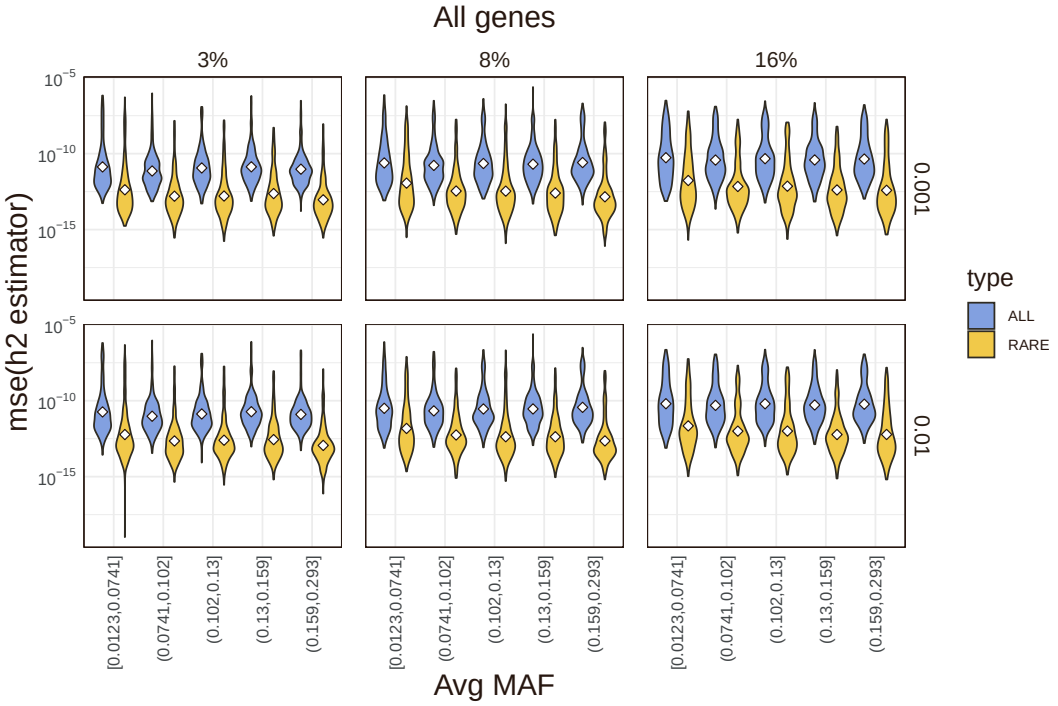

Supplementary Figure 8: MSE of $\hat{h}^2_{\text{gene,t}}$ (blue) and $\hat{h}^2_{\text{gene,r}}$ (yellow) with respect to average MAF of variants assigned to gene in simulations on chr1. Total $h^2_G = 0.05$. Cumulative $h^2_{\text{gene,t}} = 0.03$, MAF $>$ 0.005, $N = 291K$, 30 simulation replicates.

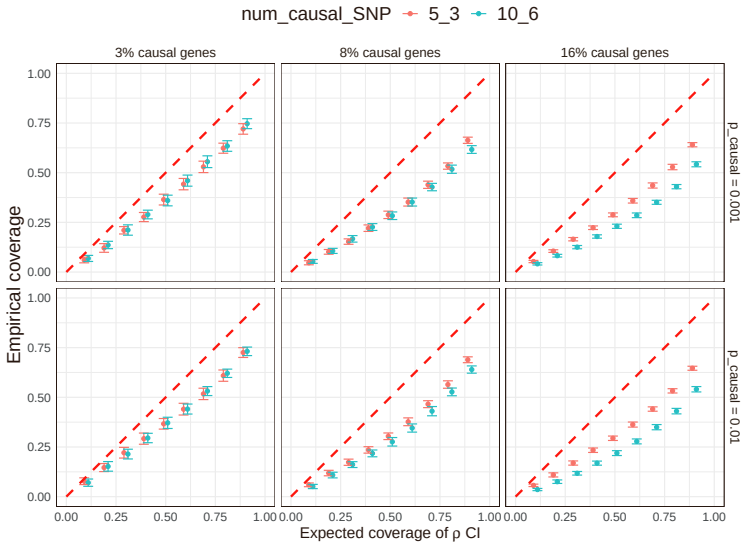

Supplementary Figure 9: Calibration of total $h^2_{\text{gene,t}}$ ρ-CIs for $\rho \in \{0.1, 0.2, ..., 0.9\}$. Empirical coverage for a given gene is the proportion of simulation replicates (out of 30) in which ρ-CI overlaps the true value of $h^2_{\text{gene,t}}$. Nonzero-h^2 genes contain either 5 (red) or 10 (blue) causal variants; their respective TSSs contain either 3 (red) or 6 (blue) causal variants (Material and Methods). Chromosome 1, MAF $>$ 0.005, N=291K, 1,083 genes.

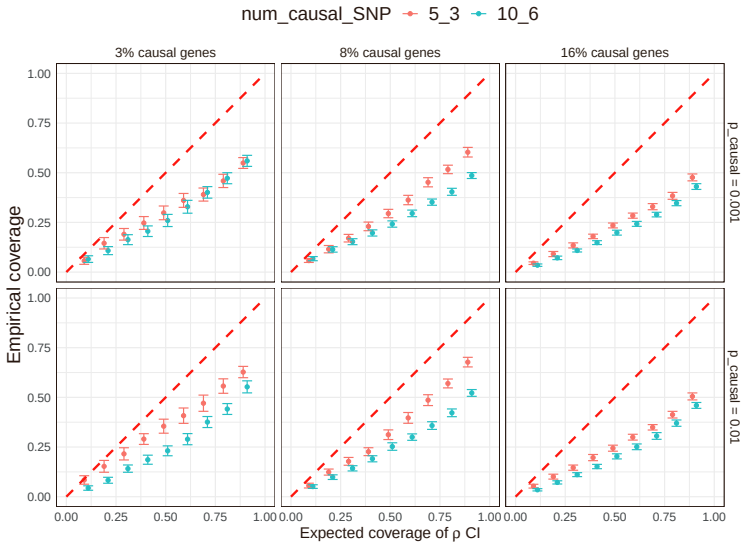

Supplementary Figure 10: Calibration of $h^2_{\text{gene,r}}$ ρ-CIs for $\rho \in \{0.1, 0.2, ..., 0.9\}$. Empirical coverage for a given gene is the proportion of simulation replicates (out of 30) in which ρ-CI overlaps the true value of $h^2_{\text{gene,r}}$. Nonzero-h^2 genes contain either 5 (red) or 10 (blue) causal variants; their respective TSSs contain either 3 (red) or 6 (blue) causal variants (Material and Methods). Chromosome 1, MAF $>$ 0.005, N=291K, 1,083 genes.

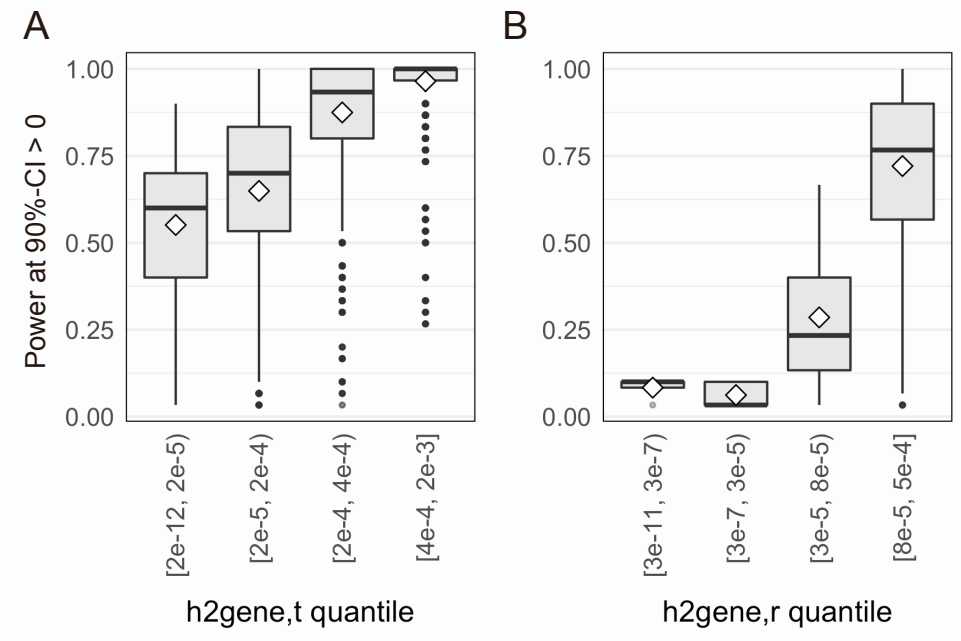

Supplementary Figure 11: Power to identify genes with (A) $h^2_{\text{gene,t}} > 0$ and (B) $h^2_{\text{gene,r}} > 0$ at the threshold 90%-CI > 0 in simulations where 16% of genes have nonzero heritability.

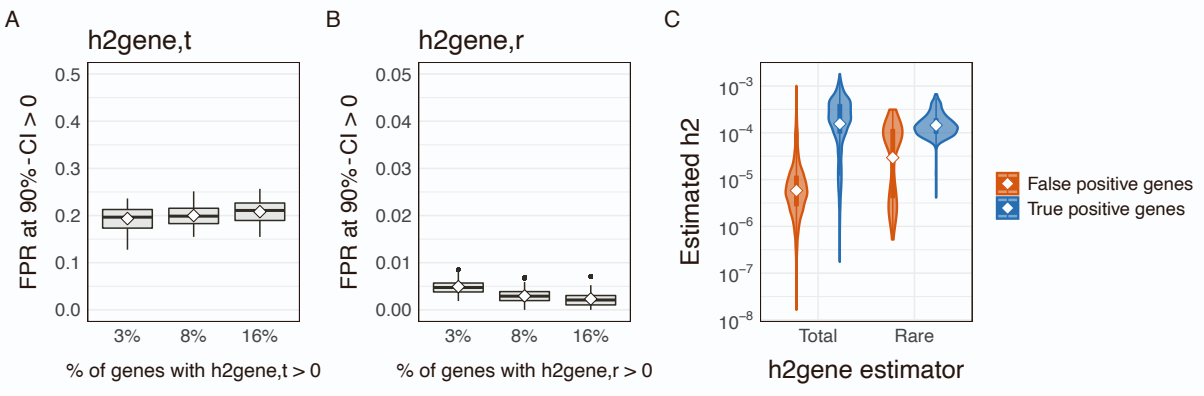

Supplementary Figure 12: False positive rate (FPR) of 90%-CI > 0 estimated from 30 simulation replicates for (A) $h^2_{\text{gene,t}}$ and (B) $h^2_{\text{gene,r}}$. (C) Distributions of estimates of $h^2_{\text{gene,t}}$ and $h^2_{\text{gene,r}}$ for true positive and false positive genes identified at 90%-CI > 0 in simulations where 16% of genes are causal. $h^2_G = 0.05$, cumulative $h^2_{\text{gene,t}} = 0.03$, MAF > 0.005, N=291K, 1,083 genes.

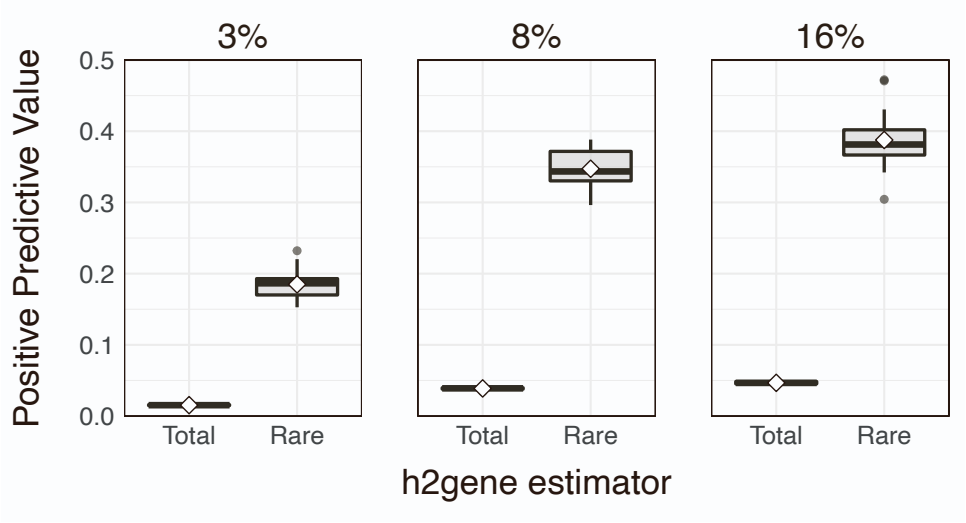

Supplementary Figure 13: Positive predictive value (PPV) for identifying genes with $(h^2_{\text{gene,r}}/h^2_{\text{gene,t}}) \geq 0.5$, using $h^2_{\text{gene,t}}$ 90%-CI > 0 or $h^2_{\text{gene,r}}$ 90%-CI > 0 as the significance threshold. For all plots: $h^2_G = 0.05$, cumulative $h^2_{\text{gene,t}} = 0.03$, MAF > 0.005, N=291K, chr1, 30 simulation replicates; white diamonds mark the mean.

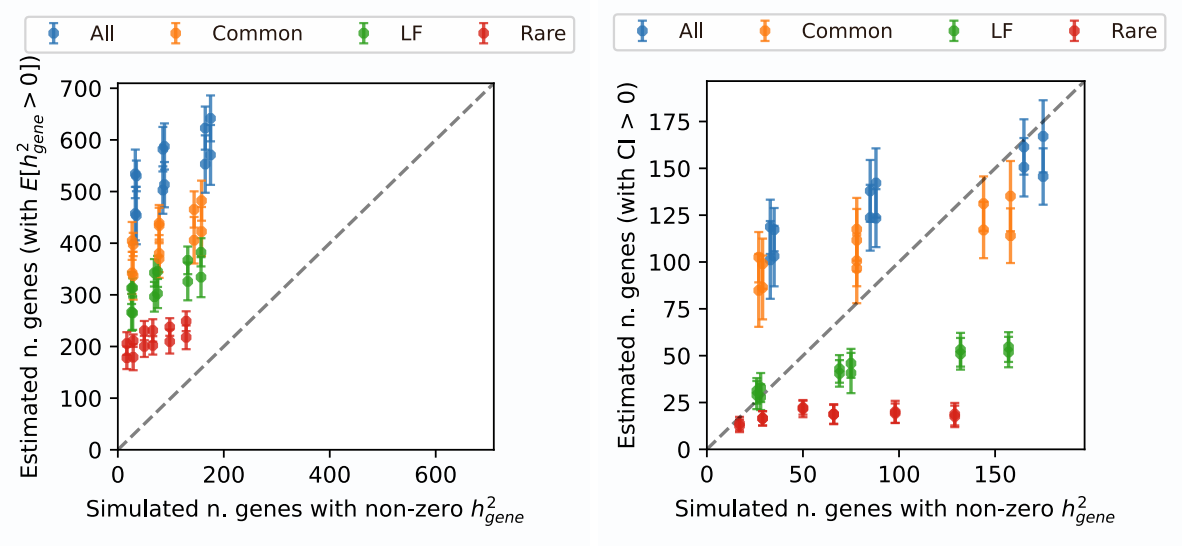

(A) Sum of per-gene posterior probabilities

(B) Number of h^2_{gene} 90%-CI > 0 genes

Supplementary Figure 14: Estimated vs. true number of nonzero-h^2 genes in simulations on chr1 ($h^2_G = 0.05$, $\sum h^2_{\text{gene,t}} = 0.03$, MAF $> 0.5\%$, N=290K). (A) For each gene, we compute the posterior probability that it has nonzero-h^2 from 500 posterior samples. The total number of nonzero-h^2 genes is then estimated by summing the posterior probabilities across genes. (B) Estimator is the number of genes with $\hat{h}^2_{\text{gene}}$ 90%-CI > 0. For both plots, each point is the average estimate from 30 simulation replicates. Error bars mark $\pm 1.96\times$SEM.

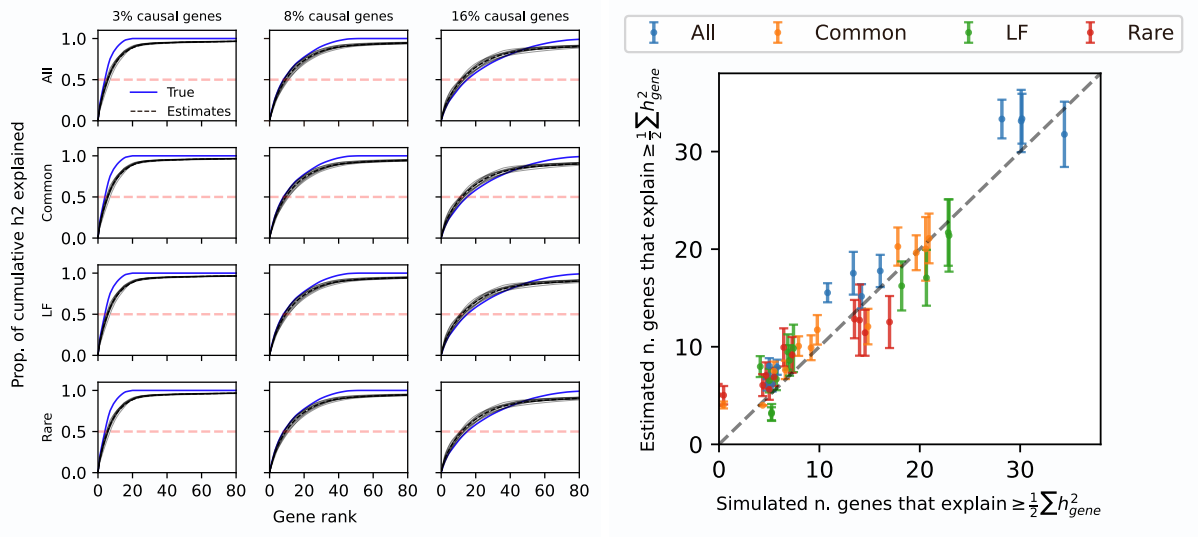

(A) (B)

Supplementary Figure 15: (A) Cumulative distributions of $h^2_{\text{gene,t}}$, $h^2_{\text{gene,c}}$, $h^2_{\text{gene,lf}}$, and $h^2_{\text{gene,r}}$ for 90%-CI > 0 genes in simulations on chr1. Each plot can be read as "top X genes with 90%-CI > 0, rank ordered by $\hat{h}^2_{\text{gene}}$ from largest to smallest, that explain Y of cumulative h^2_{gene}." (B) Estimated vs. true number of genes that explain 50% of cumulative $h^2_{\text{gene,t}}$, $h^2_{\text{gene,c}}$, $h^2_{\text{gene,lf}}$, or $h^2_{\text{gene,r}}$ in simulations. Each point is the number of genes, rank ordered by $\hat{h}_{\text{gene}}$ from largest to smallest, that explain at least 50% of cumulative gene-level h^2, averaged across 30 simulation replicates. Error bars mark $\pm 1.96\times$SEM. Simulation parameters: $h^2_G = 0.05$, $\sum h^2_{\text{gene,t}} = 0.03$, MAF $> 0.5\%$, N=290K.

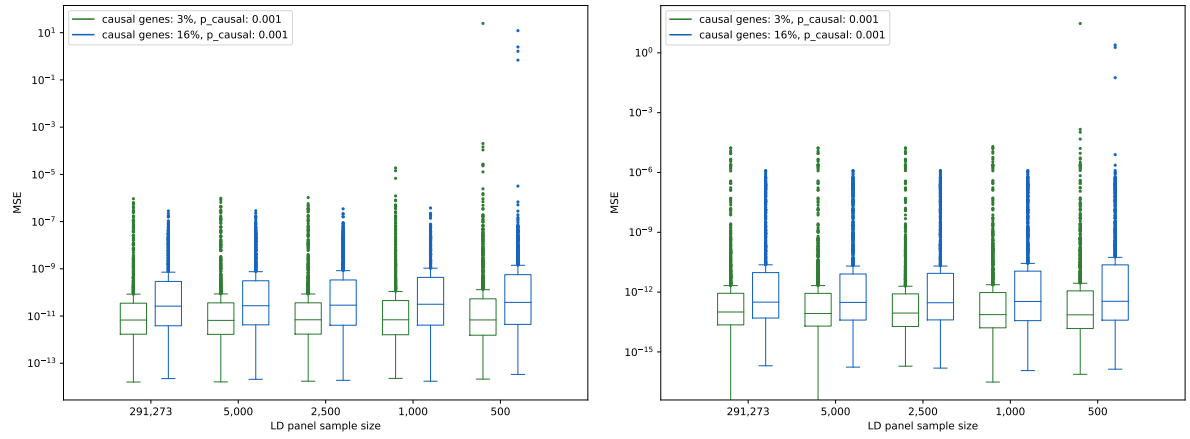

Supplementary Figure 16: MSE of $\hat{h}^2_{\text{gene,t}}$ (left) and $\hat{h}^2_{\text{gene,r}}$ (right) with respect to LD panel sample size (x-axis) in simulations (chromosome 1, MAF > 0.005, N=290K, 1,083 genes, 30 simulation replicates). Note: y-axes are different.

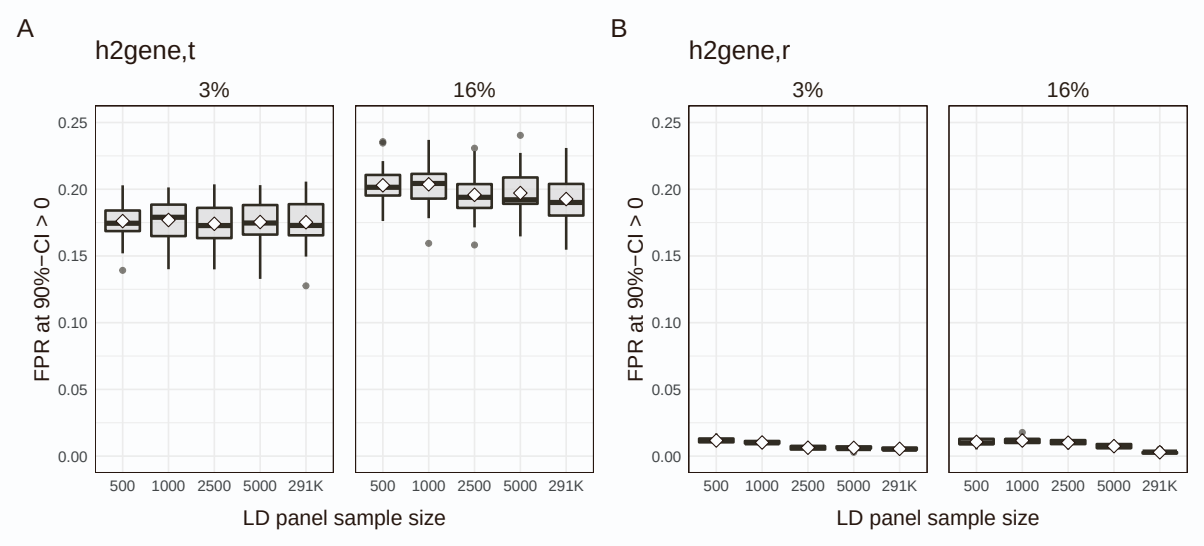

Supplementary Figure 17: False positive rate (FPR) of 90%-CI > 0 for (A) $h^2_{\text{gene,t}}$ and (B) $h^2_{\text{gene,r}}$ with respect to LD panel sample size (x-axis) in simulations (chromosome 1, MAF > 0.005, N=290K, 1,083 genes). Here, FPR is estimated as the proportion of zero-heritability genes that incorrectly pass the cutoff 90%-CI > 0 in a given simulation replicate. LD panels were generated by sampling individuals from the GWAS cohort.

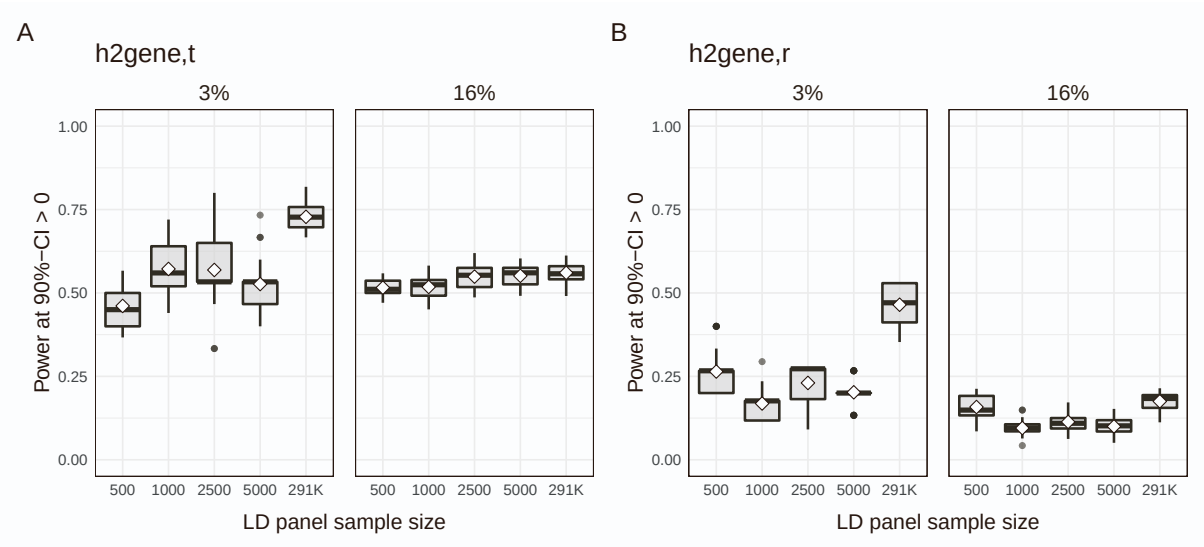

Supplementary Figure 18: Power of 90%-CI > 0 for (A) $h^2_{\text{gene,t}}$ and (B) $h^2_{\text{gene,r}}$ with respect to LD panel sample size (x-axis) in simulations (chromosome 1, MAF > 0.005, N=290K, 1,083 genes, 30 simulation replicates). Power is estimated per simulation replicate as the proportion of true nonzero-heritability genes that are correctly identified at the cutoff 90%-CI > 0. LD panels were generated by sampling individuals from the GWAS cohort.

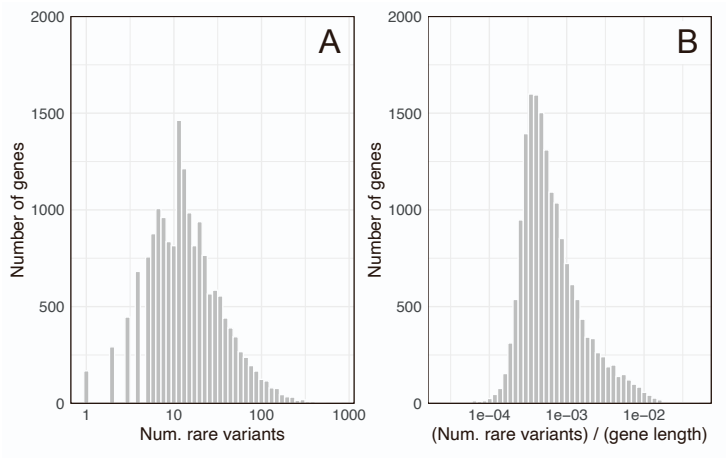

Supplementary Figure 19: Distributions of the (A) number and (B) rate of rare variants per gene body $\pm$ 10-kb upstream/downstream across 17,437 protein-coding genes.

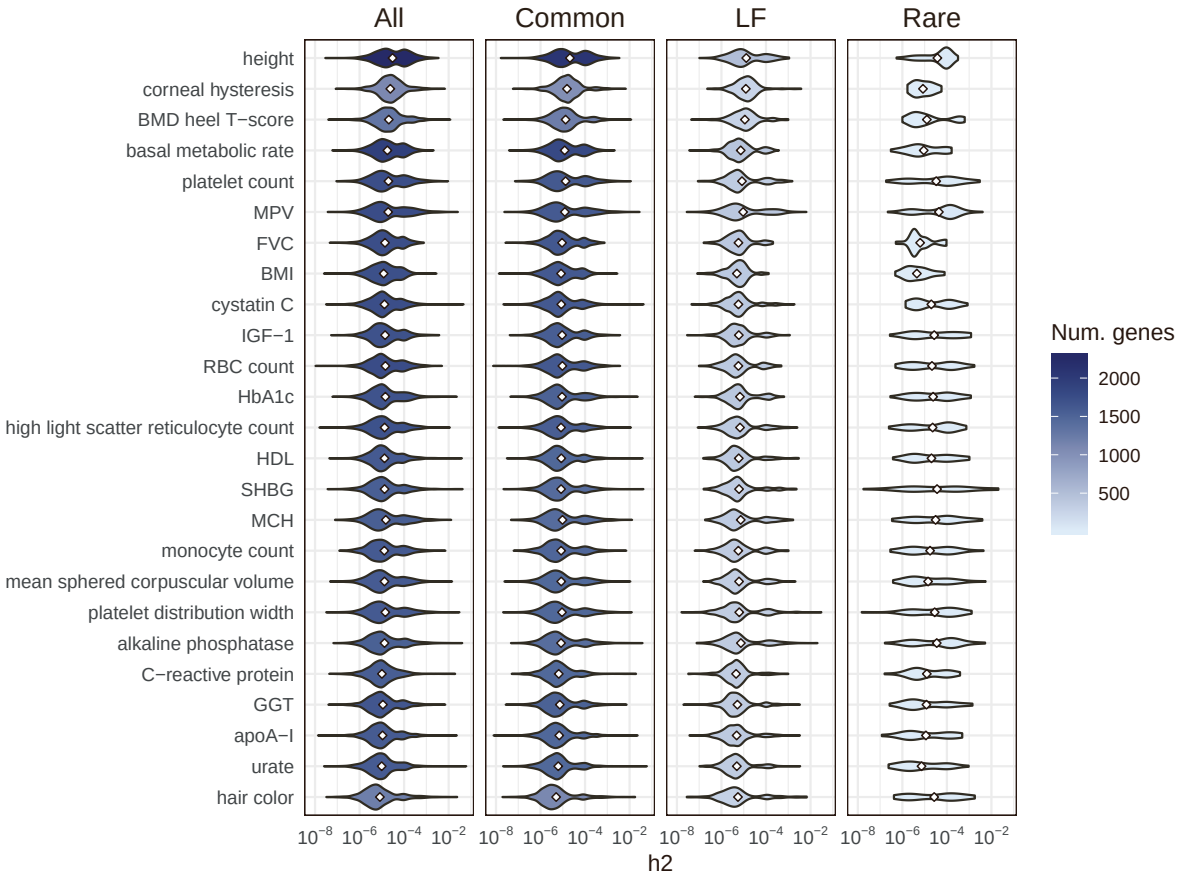

Supplementary Figure 20: Distributions of $\hat{h}^2_{\text{gene}}$ for 25 traits ($N = 290K$ "white British" individuals, UK Biobank). Each violin plot is the distribution of posterior mean estimates for genes with 90%-CI > 0 for one trait. The shading scales with the number of genes in the violin plot.

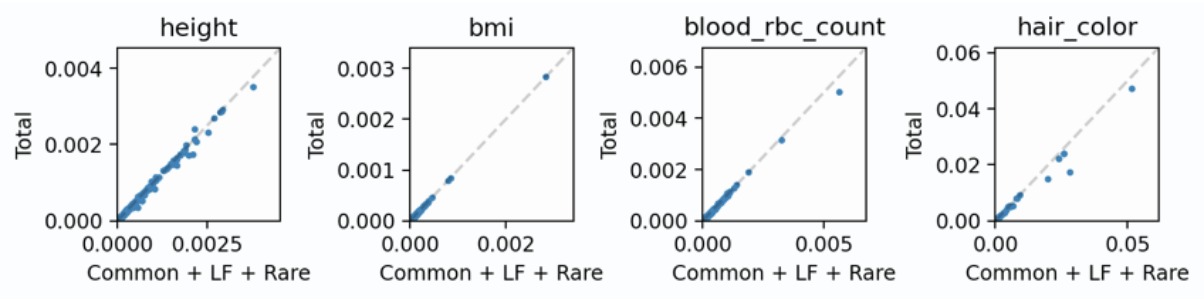

Supplementary Figure 21: $\hat{h}^2_{\text{gene,t}}$ (y-axis) vs. $\hat{h}^2_{\text{gene,c}} + \hat{h}^2_{\text{gene,lf}} + \hat{h}^2_{\text{gene,r}}$ (x-axis) across 90%-CI > 0 genes for height, BMI, red blood cell count, and hair color (N=290K, "white British," UK Biobank).

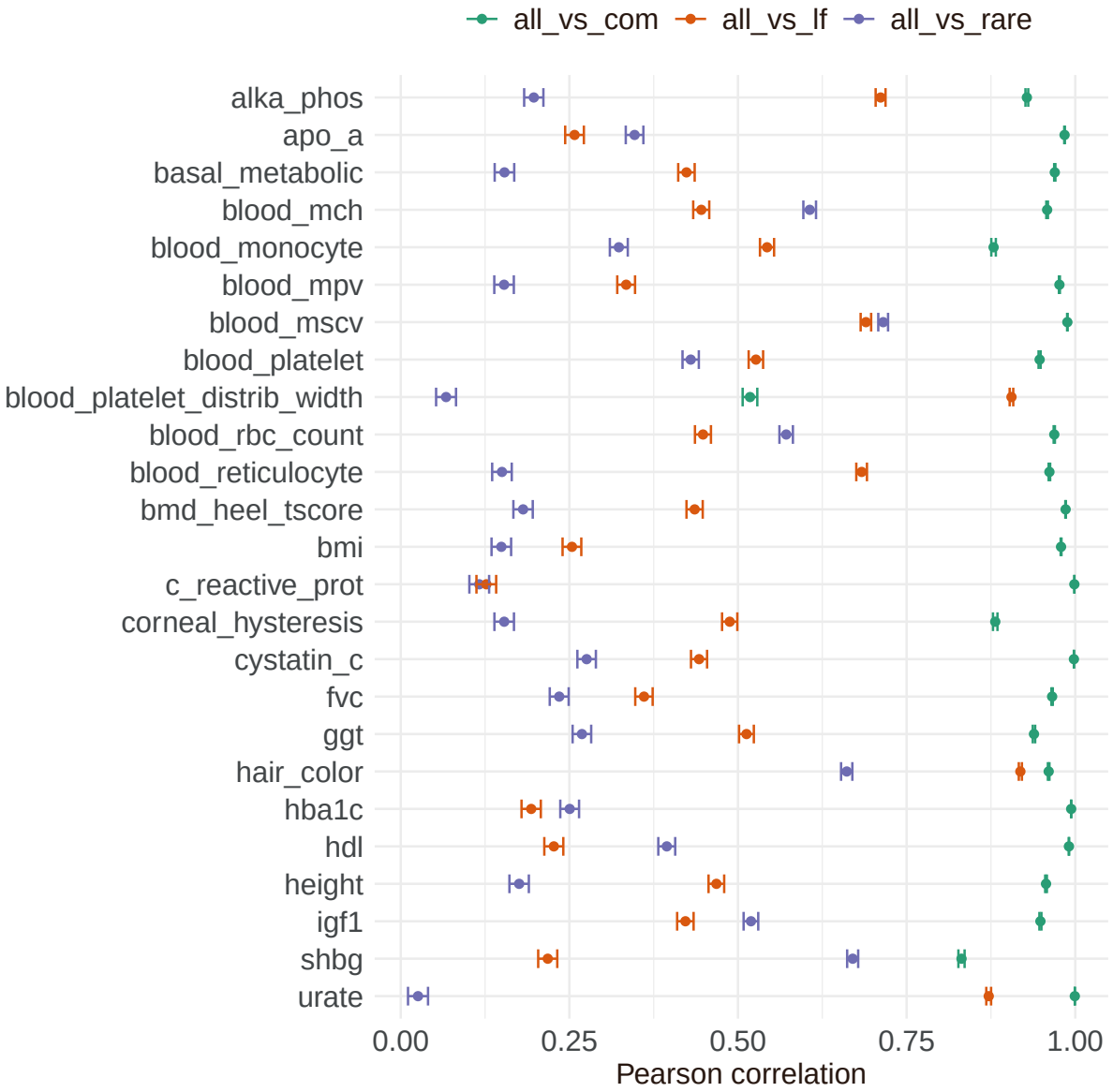

Supplementary Figure 22: Correlation of $\hat{h}^2_{\text{gene,t}}$ with $\hat{h}^2_{\text{gene,c}}$ (green), $\hat{h}^2_{\text{gene,lf}}$ (orange), and $\hat{h}^2_{\text{gene,r}}$ (purple) for 25 UK Biobank traits. Error bars mark 95% confidence intervals.

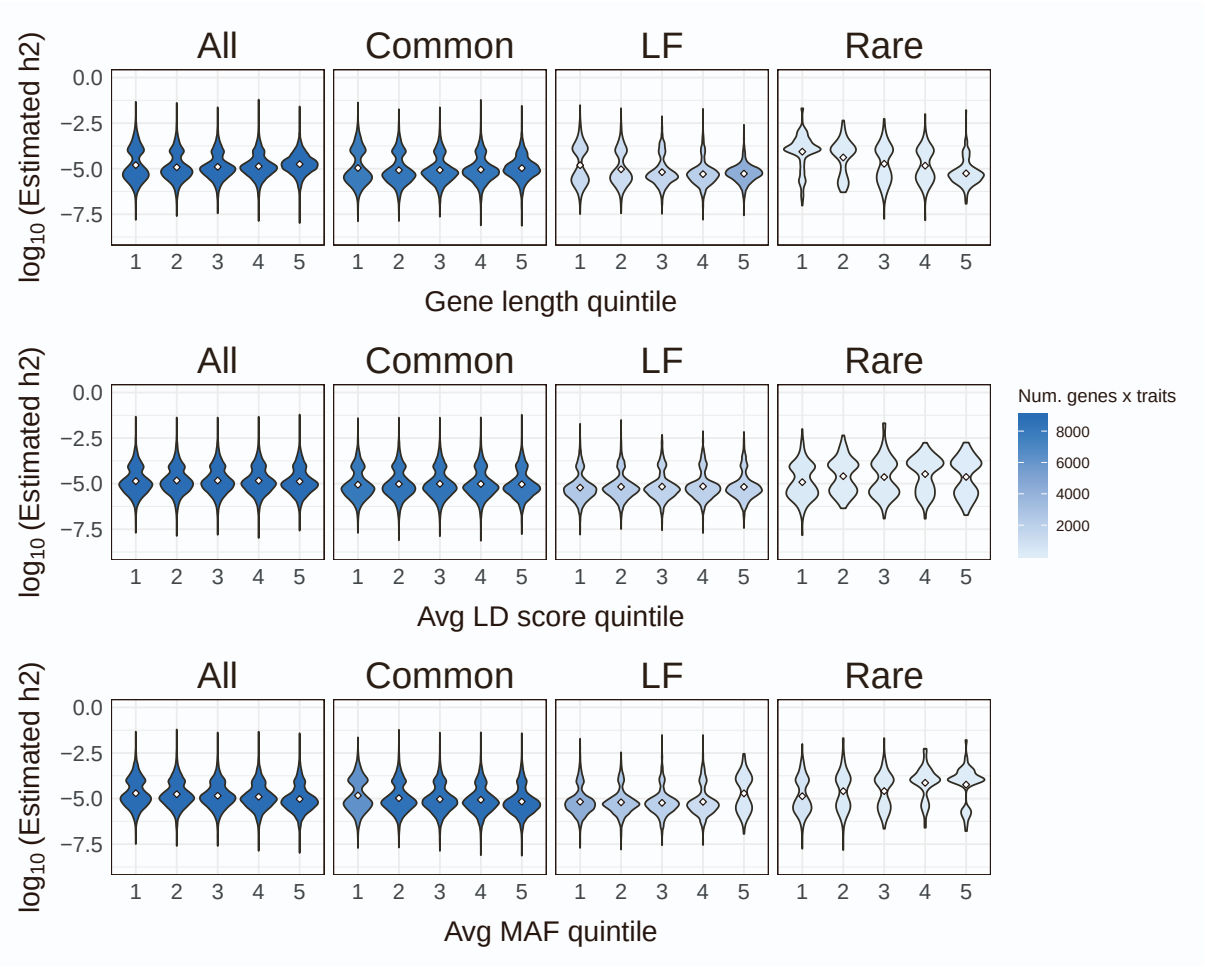

Supplementary Figure 23: Distributions of $\hat{h}^2$ for nonzero-heritability genes with respect to gene length (top), average LD score of variants assigned to gene (middle), average MAF of variants assigned to gene (bottom). Each point in each violin plot is an estimate for a unique gene-trait pair (25 traits in total). Violin plots are shaded to indicate the number of data points in the distribution. Diamonds mark the means of the distributions.

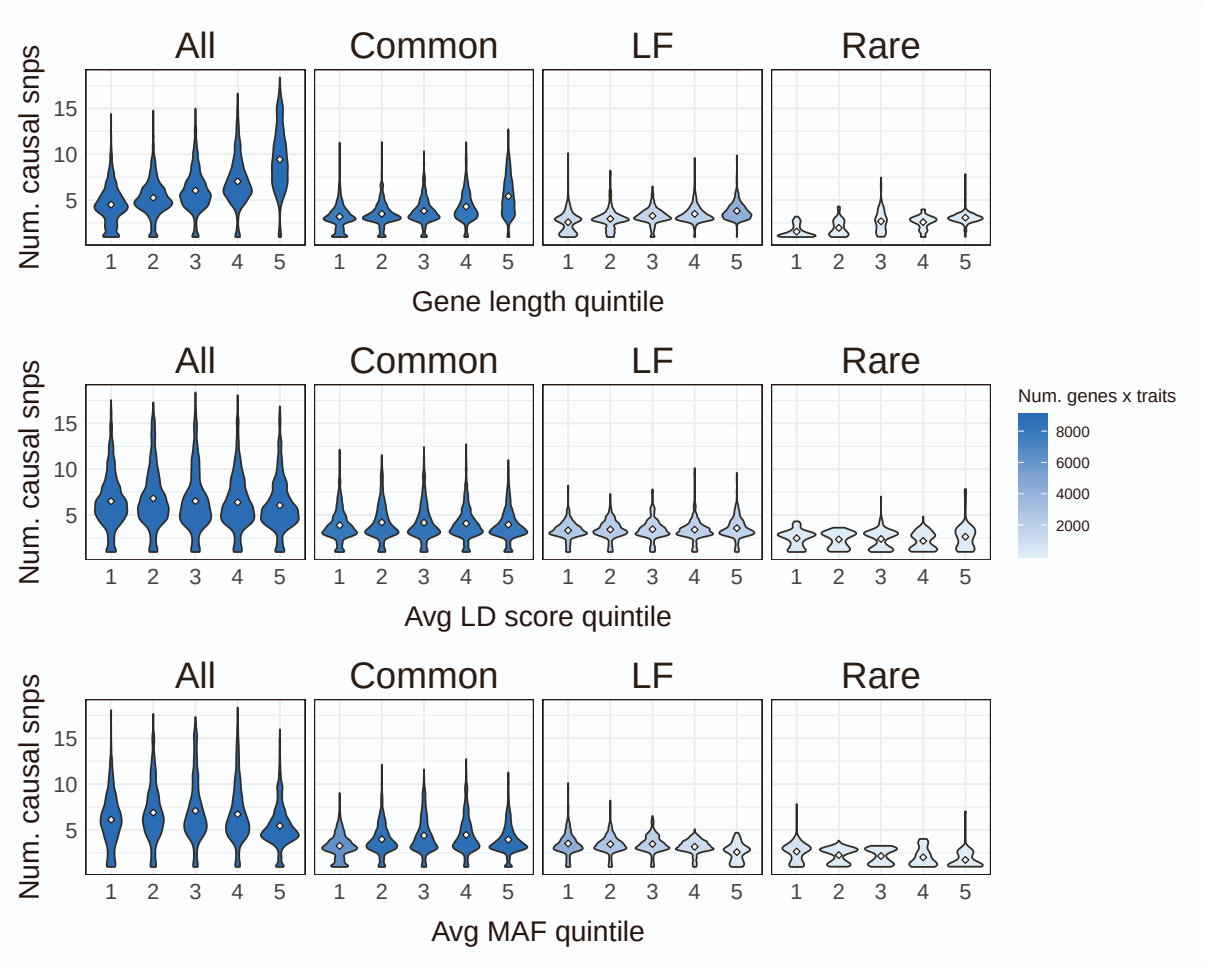

Supplementary Figure 24: Distributions of estimated number of causal variants in nonzero-heritability genes with respect to gene length (top), average LD score of variants assigned to gene (middle), and average MAF of variants assigned to gene (bottom). Violin plots are shaded to indicate the number of data points in the distribution. Each point in each violin plot is an estimate for a unique gene-trait pair (25 traits in total). Diamonds mark the means of the distributions.

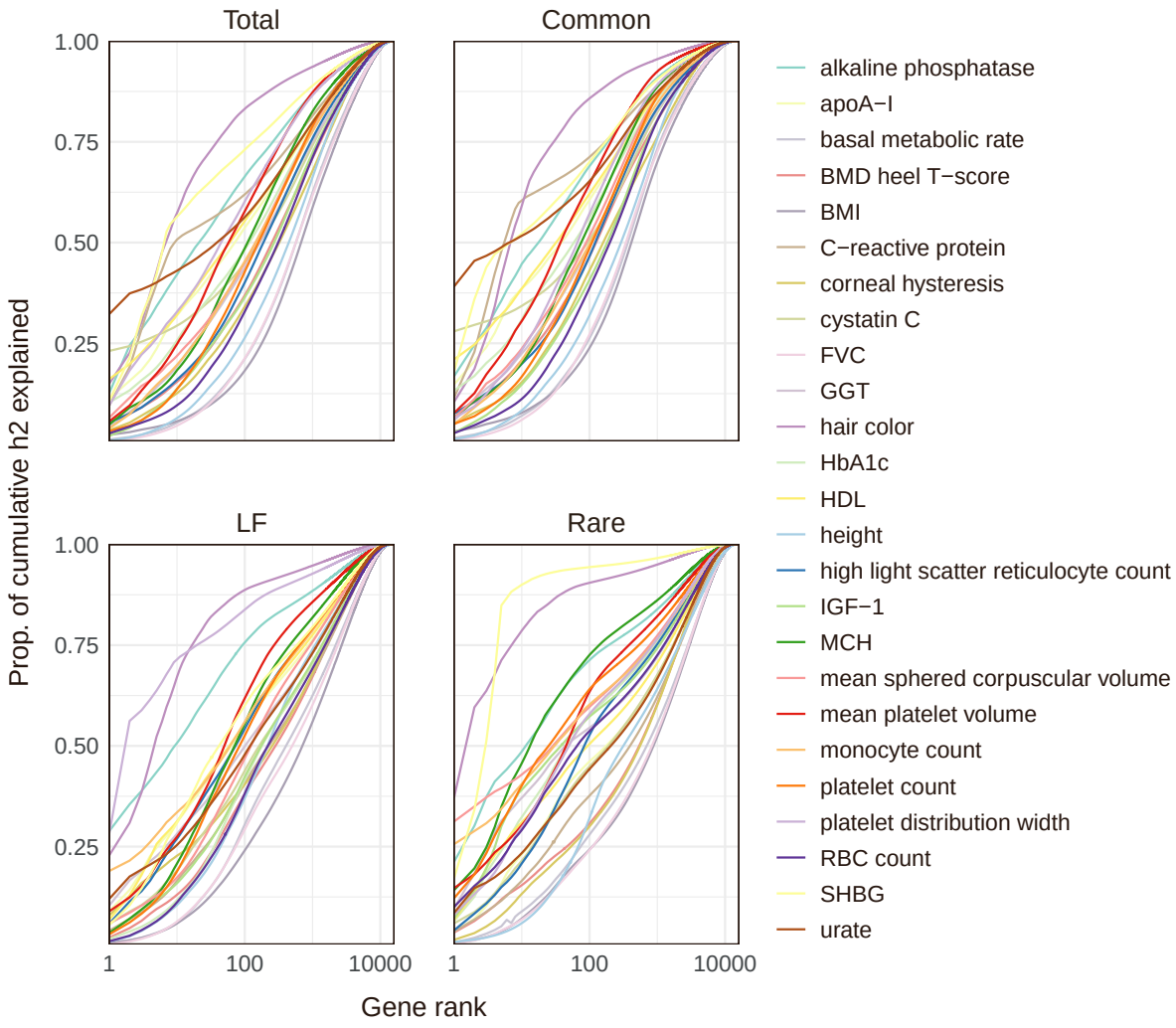

Supplementary Figure 25: Empirical cumulative distribution cumulative heritability for 25 traits. Each curve can be read as, "the top X genes explain Y% of the cumulative gene-level heritability for a given trait." Cumulative heritability is estimated as the summation of posterior mean estimates for nonzero-heritability genes (90%-CI > 0). Clockwise from the top left: $\hat{h}^{\text{“2}}_{\text{gene,t}}$, $\hat{h}^2_{\text{gene,c}}$, $\hat{h}^2_{\text{gene,r}}$, and $\hat{h}^2_{\text{gene,lf}}$.

% causal genes	p_{causal}	ρ	Underestimated		Overestimated	
			Avg num genes	Avg %	Avg num genes	Avg %
3%	0.001	0.90	6.55 (0.28)	19.29 (0.82)	2.50 (0.13)	7.37 (0.40)
3%	0.001	0.95	4.82 (0.26)	14.17 (0.78)	1.88 (0.13)	5.58 (0.40)
3%	0.01	0.90	6.25 (0.26)	18.42 (0.79)	2.98 (0.17)	8.74 (0.48)
3%	0.01	0.95	4.68 (0.23)	13.80 (0.68)	2.18 (0.14)	6.43 (0.41)
8%	0.001	0.90	25.47 (0.64)	29.39 (0.70)	5.72 (0.24)	6.62 (0.28)
8%	0.001	0.95	19.77 (0.63)	22.80 (0.70)	4.40 (0.20)	5.09 (0.23)
8%	0.01	0.90	23.13 (0.64)	26.70 (0.70)	5.93 (0.23)	6.86 (0.27)
8%	0.01	0.95	17.60 (0.58)	20.30 (0.65)	4.48 (0.24)	5.18 (0.27)
16%	0.001	0.90	61.82 (1.43)	36.22 (0.71)	7.87 (0.28)	4.62 (0.16)
16%	0.001	0.95	49.62 (1.38)	29.05 (0.71)	5.55 (0.27)	3.26 (0.15)
16%	0.01	0.90	60.55 (1.58)	35.46 (0.81)	8.83 (0.31)	5.20 (0.18)
16%	0.01	0.95	48.95 (1.47)	28.64 (0.76)	6.20 (0.27)	3.66 (0.16)

Supplementary Table 1. Calibration of h2gene ρ-CIs with respect to the number of causal genes, proportion of causal variants (p_{causal}), and $\rho \in \{0.90, 0.95\}$ in simulations (chromosome 1, MAF > 0.5%, 1,083 protein-coding genes, cumulative $h^2_{\text{gene}} = 0.03$). "Underestimated" and "overestimated" refer to genes whose ρ-CIs lie below and above their true gene-level heritability, respectively. For each simulation setup, we report the average (and s.e.m.) of the number and percentage of underestimated/overestimated genes in 30 simulation replicates.

% causal genes	p_{causal}	ρ	Underestimated		Overestimated	
			Avg num genes	Avg %	Avg num genes	Avg %
3%	0.001	0.90	9.70 (0.38)	42.41 (0.93)	0.52 (0.09)	2.15 (0.38)
3%	0.001	0.95	8.67 (0.35)	37.88 (0.95)	0.35 (0.08)	1.45 (0.31)
3%	0.01	0.90	8.98 (0.44)	38.40 (0.97)	0.67 (0.11)	2.58 (0.40)
3%	0.01	0.95	7.80 (0.40)	33.31 (1.00)	0.43 (0.09)	1.66 (0.34)
8%	0.001	0.90	25.82 (0.95)	43.76 (0.98)	1.07 (0.15)	1.78 (0.25)
8%	0.001	0.95	22.73 (0.87)	38.51 (0.95)	0.52 (0.10)	0.85 (0.16)
8%	0.01	0.90	22.97 (1.09)	38.49 (1.26)	0.87 (0.11)	1.53 (0.21)
8%	0.01	0.95	19.52 (0.95)	32.65 (1.12)	0.55 (0.09)	0.97 (0.16)
16%	0.001	0.90	61.03 (1.63)	53.38 (0.65)	1.35 (0.17)	1.27 (0.16)
16%	0.001	0.95	53.90 (1.41)	47.20 (0.60)	0.68 (0.12)	0.65 (0.12)
16%	0.01	0.90	57.87 (1.57)	50.60 (0.65)	1.27 (0.16)	1.19 (0.16)
16%	0.01	0.95	51.08 (1.36)	44.73 (0.59)	0.78 (0.12)	0.75 (0.12)

Supplementary Table 2. Calibration of h2rare ρ-CIs with respect to the number of causal genes, proportion of causal variants (p_{causal}), and $\rho \in \{0.90, 0.95\}$ in simulations (chromosome 1, MAF > 0.5%, 1,083 protein-coding genes, cumulative $h^2_{\text{gene}} = 0.03$). "Underestimated" and "overestimated" refer to genes whose ρ-CIs lie below and above their true gene-level heritability, respectively. For each simulation setup, we report the average (and s.e.m.) of the number and percentage of underestimated/overestimated genes in 30 simulation replicates.